HST/WFPC2 imaging of the QDOT ultraluminous infrared galaxy sample

Article (Published Version)

Mon. Not. R. Astron. Soc. **326,** 1333–1352 (2001)

HST/WFPC2 imaging of the QDOT ultraluminous infrared galaxy sample

D. Farrah,[1]★ M. Rowan-Robinson,[1] S. Oliver,[2] S. Serjeant,[3] K. Borne,[4] A. Lawrence,[5] R. A. Lucas,[6] H. Bushouse[6] and L. Colina[7]

[1]*Astrophysics Group, Blackett Laboratory, Imperial College, Prince Consort Road, London SW7 2BW*
[2]*Astronomy Centre, University of Sussex, Falmer, Brighton BN1 9QJ*
[3]*Unit for Space Sciences & Astrophysics, School of Physical Sciences, University of Kent at Canterbury, Canterbury, Kent, CT2 7NZ*
[4]*Raytheon ITSS, NASA GSFC, Greenbelt, MD, USA*
[5]*Institute for Astronomy, University of Edinburgh, Royal Observatory, Blackford Hill, Edinburgh, EH9 3HJ*
[6]*Space Telescope Science Institute, Baltimore, Maryland, USA*
[7]*Instituto de Fisica de Cantabria, Santander, Spain*

Accepted 2001 May 14. Received 2001 May 14; in original form 2001 February 7

ABSTRACT

We present *HST* WFPC2 *V*-band imaging for 23 ultraluminous infrared galaxies (ULIRGs) taken from the QDOT redshift survey. The fraction of sources observed to be interacting is 87 per cent. Most of the merging systems show a number of compact 'knots', whose colour and brightness differ substantially from their immediate surroundings. Colour maps for nine of the objects show a non-uniform colour structure. Features include blue regions located towards the centres of merging systems which are likely to be areas of enhanced star formation, and compact red regions which are likely to be dust shrouded starbursts or active galactic nuclei. The host galaxies of the quasi-stellar objects (QSOs) in the sample were found to be either interacting systems or ellipticals. Our data show no evidence that ULIRGs are a simple transition stage between galaxy mergers and QSOs. We propose an alternative model for ULIRGs based on the morphologies in our sample and previous *N*-body simulations. Under this model ULIRGs as a class are much more diverse than a simple transition between galaxy merger and QSO. The evolution of IR power source and merger morphology in ULIRGs is driven solely by the local environment and the morphologies of the merger progenitors.

Key words: galaxies: active – quasars: general – galaxies: Seyfert – galaxies: starburst – infrared: galaxies.

1 INTRODUCTION

The existence of galaxies that emit more radiation in the rest-frame infrared than at all other wavelengths combined was established with the first extragalactic mid-IR observations (Low & Kleinmann 1968; Rieke & Low 1972). The *Infrared Astronomical Satellite* (*IRAS*), launched in 1983, was the first observatory with sufficient sensitivity to detect these luminous infrared galaxies (LIRGs) in large numbers (Rowan-Robinson et al. 1984; Soifer et al. 1984; Sanders & Mirabel 1996). LIRGs are broadly defined as any object with $L_{\rm ir} > 10^{11}\,{\rm L}_{\odot}$.[1] These objects become the dominant extragalactic population at luminosities above $10^{11}\,{\rm L}_{\odot}$ in the local ($z < 0.5$) Universe, outnumbering Seyferts, quasi-stellar objects (QSOs) and starburst galaxies of comparable bolometric luminosity.

A subset of the *IRAS* galaxy population that has been extensively studied are the ultraluminous infrared galaxies (ULIRGs), those with $L_{\rm ir} > 10^{12}h_{65}^{-2}\,{\rm L}_{\odot}$ (or equivalently $L_{60} > 10^{11.77}h_{65}^{-2}\,{\rm L}_{\odot}$, where L_{60} is the *IRAS* 60-μm flux). Recent deep submillimetre surveys (Hughes et al. 1998; Barger, Cowie & Sanders 1999; Blain et al. 1999; Lilly et al. 1999; Peacock et al. 2000) suggest that ULIRGs are an important component of the Universe over $2 < z < 7$. The evolution of ULIRGs, their power source and the trigger mechanism behind the IR emission are still the subject of vigorous debate. Although it is now generally accepted that a mixture of star formation and active galactic nuclei (AGN) activity powers the IR emission, the *dominant* power source, and how ULIRGs evolve over time, are still unanswered questions. There are many similarities between ULIRGs and starburst galaxies (Joseph & Wright 1985; Rowan-Robinson & Crawford 1989; Condon et al. 1991). Conversely, many ULIRGs display nuclear

★E-mail: d.farrah@ic.ac.uk

[1] Where $L_{\rm ir}$ spans 8–1000μm and is computed using the flux in all four *IRAS* bands according to the prescription given by Perault (1987).

emission lines characteristic of Seyfert galaxies (Kim et al. 1995; Sanders et al. 1988). A study of 15 ULIRGs (Genzel et al. 1998) using the *Infrared Space Observatory* (*ISO*) found that the IR emission of 75 per cent was predominantly powered by star formation and 25 per cent by an AGN, although at least half the sources showed evidence for both types of emission. The spatial density, bolometric emission and luminosity function of ULIRGs are comparable to those of quasars in the local Universe. It has been suggested (Sanders et al. 1988) that ULIRGs represent the dust-enshrouded precursors to optically selected QSOs and that all QSOs emerge from a luminous infrared phase. The majority of ULIRGs appear to lie in interacting or merging systems, although the exact fraction is still not certain (Sanders et al. 1988; Leech et al. 1994; Clements et al. 1996a). A merger would provide an ideal environment for triggering a nuclear starburst or AGN and thus would be a possible triggering mechanism for QSOs. A merger between two spirals is also likely to form an elliptical galaxy (Barnes 1989), therefore ULIRGs may also have a pivotal role to play in elliptical galaxy evolution (Kormendy & Sanders 1992). The relation of ULIRGs to their higher luminosity counterparts, hyperluminous infrared galaxies (HLIRGs, those with $L_{\rm ir} > 10^{13} h_{65}^{-2}\,{\rm L}_{\odot}$) is also not fully understood (Hines et al. 1995; Rowan-Robinson 2000). Although HLIRGs as a class appear to be an extrapolation of ULIRGs to extreme luminosities, there exists the possibility that some fraction of HLIRGs are an entirely different population (Farrah et al. 2001).

In this paper we present *Hubble Space Telescope* (*HST*) images, taken with the F606W filter using the Planetary Camera (PC) on Wide Field Planetary Camera 2 (WFPC2), for 23 ULIRGs and compare them to WFPC2 WF3 F814W band data for 22 of these sources. Sample selection and observations are described in Section 2. Data reduction, photometry, colour map construction and point spread function (PSF) subtraction are described in Section 3. Results are presented in Section 4. Discussion of the results can be found in Section 5 and conclusions are summarized in Section 6.

We have taken $H_0 = 65\,{\rm km\,s^{-1}\,Mpc^{-1}}$, $\Omega_0 = 1.0$ and $\Lambda = 0$ unless otherwise stated.

2 SAMPLE

2.1 Sample selection

The 23 galaxies in our sample are randomly selected from those ULIRGs discovered in the QDOT all sky *IRAS* galaxy redshift survey (Lawrence et al. 1999). This survey consists of an all sky sample of 2387 *IRAS* galaxies brighter than the *IRAS* PSC 60-μm completeness limit of 0.6 Jy, and is complete to greater than 98 per cent. All the galaxies in our sample have 60-μm luminosities in the range $10^{11.77}$–$10^{12.50} h_{65}^{-2}\,{\rm L}_{\odot}$. The redshift range is $0.14 < z < 0.35$ with a median redshift of $z = 0.18$ and a mean redshift of $z = 0.20$.

2.2 Observations

The data were taken in cycle 8 between 1998 October and 1999 July using the WFPC2. The coordinates of each source were centred on the PC charge-coupled device (CCD), selected for its superior pixel scale [$0.046\,{\rm arcsec\,pixel^{-1}}$ as opposed to $\sim 0.1\,{\rm arcsec\,pixel^{-1}}$ for the Wide Field Camera (WFC)] and full sampling of the PSF over the WFC CCDs. At the mean redshift of our sample the pixel scale of the PC corresponds to a physical size of 0.2 kpc. Exposures were taken using the F606W filter, which corresponds approximately to the *V*-band filter in the Cousins system. The observations were performed in 'snapshot' mode, each object being imaged for 600 s. Each observation was split into two exposures of 300 s to facilitate the subtraction of cosmic rays.

For 22/23 of the sample, data were taken using the WFC 3 CCD and the wide band F814W filter, which corresponds closely to the *I*-band filter in the Cousins system, as part of a separate program (prop. ID 6346, PI K. Borne). These observations were also taken in 'snapshot' mode, each object being imaged for 800 s.

The conversion between *HST* filter system magnitudes and Cousins magnitudes is not straightforward. Depending on the filter used for the observations the applied conversion factor can be strongly related to the object spectrum. For the F606W filter the dependence of the conversion factor to Cousins *V* band on the object spectrum is quite large, and can introduce photometric errors of $\Delta m = 0.2$ or more. For the conversion between F814W magnitudes and Cousins *I* band the dependence is much smaller, generally $\Delta m < 0.05$. In order to avoid these associated uncertainties, magnitudes are given in the *HST* filter system using the VEGAMAG synthetic zero-points (Holtzman et al. 1995), and have not been converted into the Cousins filter system. The differences between our F814W magnitudes and the equivalent Cousins *I*-band magnitudes are likely to be very small, with $\Delta m < 0.1$. For the F606W filter, which is both wider and redder than the *V*-band Cousins filter, the match is much poorer. Hence we do not make comparisons between our F606W band magnitudes and previously quoted *V*-band magnitudes, but do make comparisons between our F814W band magnitudes and previously quoted Cousins *I*-band magnitudes.

3 DATA ANALYSIS

3.1 Data reduction

Upon arrival all data sets were recalibrated with the best available reference files, using the IRAF task CALWP2, and combined into a single image using the IRAF task CRREJ. Following sky subtraction, warm pixels were removed by linear interpolation from their immediate neighbours. Photometric solutions were calculated using the SYNPHOT package from the Space Telescope Science Institute (STScI), recently updated to match the solutions given by Holtzman et al. (1995). For those QSOs in the sample that were saturated in the central regions, magnitudes and fluxes were computed using PSF fitting photometry. Corrections were made for detector gain (for these observations the gain was $7{\rm e}^{-}/DN$) and aperture size. Absolute magnitudes were derived using the expression:

$$M = m - 25 - 5\log(2c/100h)(1+z)[1-(1+z)^{-1/2}] \qquad (1)$$

We estimate that our derived relative magnitudes have an associated photometric error of approximately 4 per cent. Fluxes in Jy were obtained by multiplying the flux in $\rm ergs\,cm^{-2}\,s^{-1}\,\AA^{-1}$ by the central wavelength of the F814W filter in angstroms, and then dividing by the central wavelength in Hz. As such they do not include any bandpass correction.

No *k*-corrections have been applied to the calculated absolute magnitudes. Trial *k*-corrections for both the F606W and F814W filters were computed using the spectral synthesis package PEGASE (Fioc & Rocca-Volmerange 1997). At the mean redshift of the sample, $z = 0.2$, the *k*-correction in the F606W band was found to be of the order $\Delta m = 0.15$ for a 10^9 yr old spiral galaxy, with the correction in the F814W filter being slightly lower. Even at the highest redshift in the sample, $z = 0.345$, the *k*-correction was not much greater than this ($\Delta m = 0.18$). It was found that, if the age of

the system was varied across 10^7–10^{10} yr and/or a different source spectrum was assumed, then the computed *k*-correction varied across the range $-0.02 < \Delta m < 0.3$. The errors introduced in applying these synthetic *k*-corrections therefore probably significantly outweigh any corrective effect. There are also no applied corrections for reddening due to dust extinction.

3.2 Colour maps

Colour maps are an invaluable tool for highlighting morphological features not apparent in single band images. Constructing colour maps for the F606W and F814W band data presented here is not straightforward as the data were taken on different CCDs. The PSF for any of the WFPC2 CCDs is strongly dependent on position, wavelength, and CCD characteristics. These differences must be carefully accounted for when matching the two images.

The F606W and F814W band images were first scaled to a common exposure time and gain. Although the readout noise does not scale linearly for the PC and WF3 chips, this effect is not significant when the exposure time of one image is at least 10 per cent of the other. Following the advice of the STScI, the images were then deconvolved with appropriate PSFs using the Richardson–Lucy algorithm (Lucy 1974) as implemented in the IRAF task LUCY. The TinyTIM v5.0 software (Krist 1995) was used to generate PSFs for the appropriate filter and chip positions. The four frames in the F606W and F814W observations were then combined into single images using the IRAF task WMOSAIC, which corrects for geometric distortion, offsets and scale differences between the PC and the WFCs. This task also degrades the PC *V*-band images to the resolution of the Wide Field Cameras, effectively convolving the PC image. Any residual PSF mismatch is thus due to differences in the effective PSFs of the images achieved by the initial deconvolutions. Since this PSF mismatch could in principle be significant we performed simulations to assess the accuracy of this procedure by constructing colour maps of stars visible in both the PC and WFC CCDs. It was found that the maps of these stars had a featureless colour structure. Although some level of PSF mismatch is undoubtedly still present it appears to be negligible compared to noise in the original images or large angle scattering within the WFPC2 optics.

A further potential source of extraneous colour structure with this method is that of deconvolution artefacts. These can include sharp colour peaks caused by amplification of poisson noise in the original images, or very bright point sources surrounded by dark rings which are caused by large numbers of iterations on a bright point source within an envelope of extended emission. To minimize the occurrence of these artefacts we examined the images after each iteration. It was found that deconvolution artefacts only became visible several iterations after convergence between the original image and the deconvolved image had been achieved (measured via a reduced χ^2 statistic). As we halted the deconvolution immediately upon attaining convergence, the effect of artefacts on the achieved colour structure is insignificant.

3.3 QSO host galaxies

Host galaxies can only be resolved in QSOs if light from the central bright source and from the host galaxy can be separated. The most convenient way to accomplish this is by fitting a point-source template to the QSO, the template being established from a set of observations of stellar PSFs that are a good match in colour, filter and detector position to the targets. For the optical QSOs in this sample no additional observations were made of nearby stars, and no suitable observed PSFs were available in the *HST* PSF archive. Synthetic PSFs were therefore generated using TinyTIM.

Ten times oversampled PSFs were generated. These PSFs were then shifted by non-integer pixel distances, rebinned to PC resolution and convolved with the PC pixel scattering function. The agreement between these synthetic PSFs and observed (stellar) PSFs is generally excellent within radii of about 2 arcsec. Beyond this radius scattered light in the WFPC2 optics can have a significant effect, an effect that is not modelled by the TinyTIM software. The effect of any systematic uncertainties in the PSF has also not been examined, such effects are however likely to be negligible.

The resulting PSFs were then centroided and normalized to the image via a reduced χ^2 fit. It was found that all the QSO images were saturated in the central regions to varying extents, mostly confined to the central 3×3 pixels and never beyond the central 5×5 pixels. In all cases the centralmost possible pixels were used, avoiding those that were saturated or that lay in the diffraction spikes. This method allows the image and PSF to be registered to within ~ 0.2 pixels (estimated by visual inspection), and also gives a starting value for the PSF normalization.

3.4 Profile fitting

In order to determine the morphology of the host galaxies of the QSOs in the sample, both de Vaucoleurs and exponential disc profiles were fitted to the surface brightness profiles of the host galaxies. The de Vaucoleurs profile is of the form:

$$I(r) = I_0 \, \mathrm{e}^{-7.67[(r/r_e)^{1/4}-1]} \tag{2}$$

and the exponential disc profile is of the form:

$$I(r) = I_0 \, \mathrm{e}^{-(r/h)} \tag{3}$$

One-dimensional surface brightness profiles of the sources were extracted by fitting annuli spaced at 1-pixel intervals, fixing the ellipticity (at $\epsilon = 0.05$), semimajor axis and position angle for each fit. The PSF profile together with either a radial de Vaucoleur or disc profile were then fitted to the source surface brightness profile, treating the PSF normalization as a third free parameter. This helps to minimize as far as possible the systematic errors introduced by subtracting off a 'best guess' PSF and fitting a galaxy profile to the remaining light distribution. Fitting was carried out using Levenberg–Marquardt least-squares minimization in order to derive robustly the best-fitting parameters. Two-dimensional isophote fitting, using the IRAF task ELLIPSE, was also used to investigate the ellipticities and isophotal twisting (large changes in azimuthal angle as a function of radial position) for each host by iteratively fitting isophotes of constant surface brightness whilst allowing the ellipticity and position angle to vary.

In order to quantify whether a host galaxy was detected or not we imposed the condition that a PSF + galaxy to QSO fit must be better than a pure PSF fit to at least 99 per cent confidence, computed via an *F* test. We excluded pixels within the central 0.2 arcsec as the PSF within this radius is highly undersampled. We also excluded all pixels beyond 2 arcsec because of light scattered within the WFPC2 optics.

4 RESULTS

4.1 Morphology and colours

Positions, redshifts, magnitudes, spectral types, luminosities and

Table 1. Ultraluminous QDOT galaxies observed by *HST*.

Name	RA (2000)	Dec (2000)	z	Type[a]	L_{60}[b]	L_V[c]	m_{606}	M_{606}	M_{814}[d]	$f_{25}f_{60}$[e]	Class.[f]	A[g]
	h m s	° ′ ″										
00275−2859	00 30 04.1	−28 42 24.3	0.280	Sy1	12.30	11.34	16.63	−24.06	−24.76	0.25	6/C	0.398
02054+0835	02 08 06.9	08 50 04.6	0.345	Sy1	12.48	11.11	17.69	−23.48	−24.49	<0.417	1/C	0.242
02587−6336	02 59 43.2	−63 25 03.4	0.255	Sb	12.24	10.46	18.62	−21.85	−23.10	0.123	4/A	0.277
04384−4848	04 39 50.9	−48 43 16.5	0.204	Sb	12.21	10.56	17.83	−22.13	−22.89	0.07	6/B	0.381
06268+3509	06 30 13.3	35 07 49.1	0.170	Sb	12.00	10.61	17.32	−22.24	−23.18	<0.27	6/A	0.414
06361−6217	06 36 35.9	−62 20 32.4	0.160	Sb	12.19	10.34	17.84	−21.58	−22.45	0.10	6/B	0.335
06561+1902	06 59 05.7	18 58 20.3	0.188	Sb	12.11	10.46	17.93	−21.86	−23.04	<0.27	5/A	0.252
07381+3215	07 41 21.3	32 08 23.9	0.170	Sb	11.90	10.10	18.57	−20.98	−22.37	<0.20	6/B	0.333
10026+4347	10 05 42.0	43 32 40.8	0.178	Sy1	11.85	11.07	16.28	−23.39	−23.81	0.33	0/C	0.330
10579+0438	11 00 33.8	04 22 08.2	0.173	Sb	11.84	10.14	18.54	−21.06	−22.06	<0.44	6/B	0.272
13469+5833	13 48 40.3	58 18 52.2	0.158	H II	12.08	10.51	17.39	−22.00	−23.17	<0.06	6/B	0.438
14337−4134	14 36 59.2	−41 47 06.6	0.182	Sb	11.87	10.42	17.95	−21.76	−22.86	<0.42	6/B	0.399
16159−0402	16 18 36.5	−04 09 42.8	0.213	Sb	12.22	10.50	18.09	−21.97	−23.16	0.31	6/B	0.484
17431−5157	17 47 09.9	−51 58 46.3	0.175	LINER	11.85	9.98	18.96	−20.66	−22.15	<0.38	4/B	0.283
18520−5048	18 55 59.1	−50 44 53.2	0.152	Sb	11.78	10.51	17.30	−22.00	–	<0.23	5/A	0.434
18580+6527	18 58 14.0	65 31 26.4	0.176	Sb/Sy2	11.97	11.24	15.81	−23.82	−24.52	0.09	6/B	0.587
20037−1547	20 06 31.9	−15 39 06.7	0.192	Sy1	12.36	11.25	16.00	−23.82	−24.44	<0.17	5/C	0.483
20109−3003	20 14 05.6	−29 53 52.7	0.143	Sb	11.83	10.48	17.26	−21.91	−22.67	<0.28	6/B	0.295
20176−4756	20 21 11.0	−47 47 08.6	0.178	Sb	11.98	10.44	17.84	−21.81	−23.11	<0.08	4/A	0.252
20253−3757	20 28 37.5	−37 47 10.2	0.180	Sb	11.93	10.61	17.44	−22.24	−23.28	<0.40	5/A	0.462
20507−5412	20 54 25.5	−54 01 13.7	0.228	Sb	12.05	10.20	18.98	−21.23	−22.29	<0.15	6/B	0.313
23140+0348	23 16 35.2	04 05 18.8	0.220	BLRG	12.02	10.85	17.29	−22.85	−23.84	<0.31	0/B	0.215
23220+2919	23 24 27.9	29 35 40.3	0.240	HX	12.27	10.33	18.79	−21.54	−22.51	<0.15	6/B	0.307

Coordinates and V-band magnitudes are taken from the *HST* PC images and are in the *HST* flight filter system.
[a]Spectral classification, taken from Lawrence et al. 1999 and the NASA/IPAC Extragalactic Database: 'Sb' – Starburst, 'Sy1/Sy2' – Seyfert 1/2, 'BLRG' – Broad Line Radio Galaxy, 'HX' – High Excitation but not Seyfert 2.
[b]60-μm luminosity taken from Lawrence et al. 1999 and converted to $H_0 = 65$, $\Omega_0 = 1$.
[c]Logarithm of the F606W band luminosity, computed from the F606W band images and in units of bolometric solar luminosities (3.823×10^{33} ergs s^{-1}).
[d]As measured from the WF3 F814W band images, but see also Borne et al.
[e]*IRAS* 25–60-μm flux ratio.
[f]First number is from the seven band system presented in Lawrence et al. 1989 and described in Section 4.1., second letter is from the three band system described in Section 4.1.
[g]Asymmetry statistic, computed using equation (4) and described in Section 4.1

Table 2. Binary system magnitudes.

Source	RA	Dec	M_V	M_I
02587−4336 *A*	$59^m43^s.07$	$25'05''.43$	−20.50	−21.50
02587−4336 *B*	$59^m43^s.48$	$25'00''.88$	−21.62	−22.81
20176−4756 *A*	$21^m10^s.67$	$47'08''.12$	−20.97	−22.16
20176−4756 *B*	$21^m11^s.44$	$47'09''.16$	−21.45	−22.52

Coordinates are J2000.

merger classification for the sample can be found in Table 1. The *HST* PC images of the sample can be found in Figs 1–4. For the two binary systems where the galaxies are clearly separated the magnitude of both sources together is given. Magnitudes of individual galaxies in binary systems can be found in Table 2.

Contributions to the measured magnitudes from emission lines could in principle be significant, as many ULIRGs are known to be strong emission line galaxies (Veilleux, Kim & Sanders 1999). At the mean redshift of our sample the Hα lies near the centre of the F814W bandpass, and the O III line lies nearly in the centre of the F606W bandpass. We evaluated uncertainties in our measured magnitudes by comparison with Hα and O III luminosities taken from Veilleux et al. (1999). The F606W band luminosities of our sample span the range $10.0 < L_V < 11.4$, with all but three having $L_V > 10.3$ (where L_V is the logarithm of the F606W band luminosity in units of bolometric solar luminosities). The F814W band luminosities, although not quoted in Table 1, span a similar range. In contrast, the dereddened Hα luminosities from Veilleux et al. (1999) lie in the range $7.0 < L_{H\alpha} < 10.5$, with most lying in the range $8.0 < L_{H\alpha} < 9.3$. Similarly, the O III luminosities span the range $7.0 < L_{O\,III} < 10.0$, with most falling between $7.0 < L_{O\,III} < 8.0$. The uncertainty in our quoted magnitudes and colours due to these emission lines is therefore almost certainly much less than $\Delta m = 0.1$ for all the objects in the sample.

In order to provide a quantitative description of the morphologies in the sample we have classified the sources according to the seven band prescription given by Lawrence et al. (1989):

0: Source has no companions within 200 kpc and shows no signs of interaction or merger.

1: Source has a faint companion (between 4 and 2 mag fainter than the source) between 40 and 200 kpc away.

2: Source has a bright companion (less than 2 mag fainter than the source) between 40 and 200 kpc away.

3: Source has a faint companion less than 40 kpc away but shows no signs of interaction.

4: Source has a bright companion less than 40 kpc away but shows no signs of interaction.

5: Source is interacting with companion, and there are signs of tails, loops, or bridges.

6: Source is merging; either there is obvious disturbance and/or there are two or more nuclei in a common envelope.

No source in the sample is an isolated undisturbed spiral or

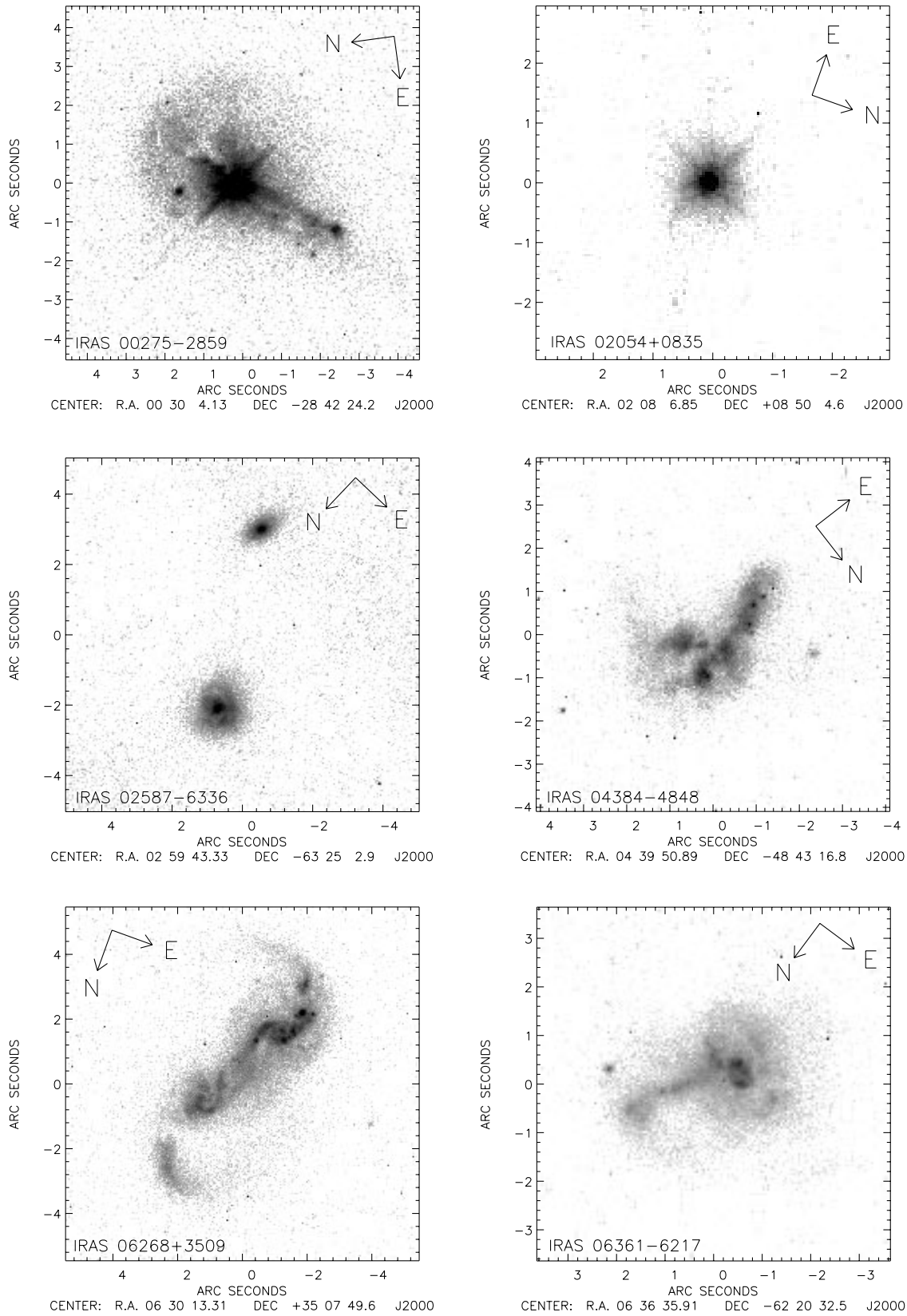

Figure 1. *HST* F606W images of IRAS 00275−2859 to IRAS 06361−6217.

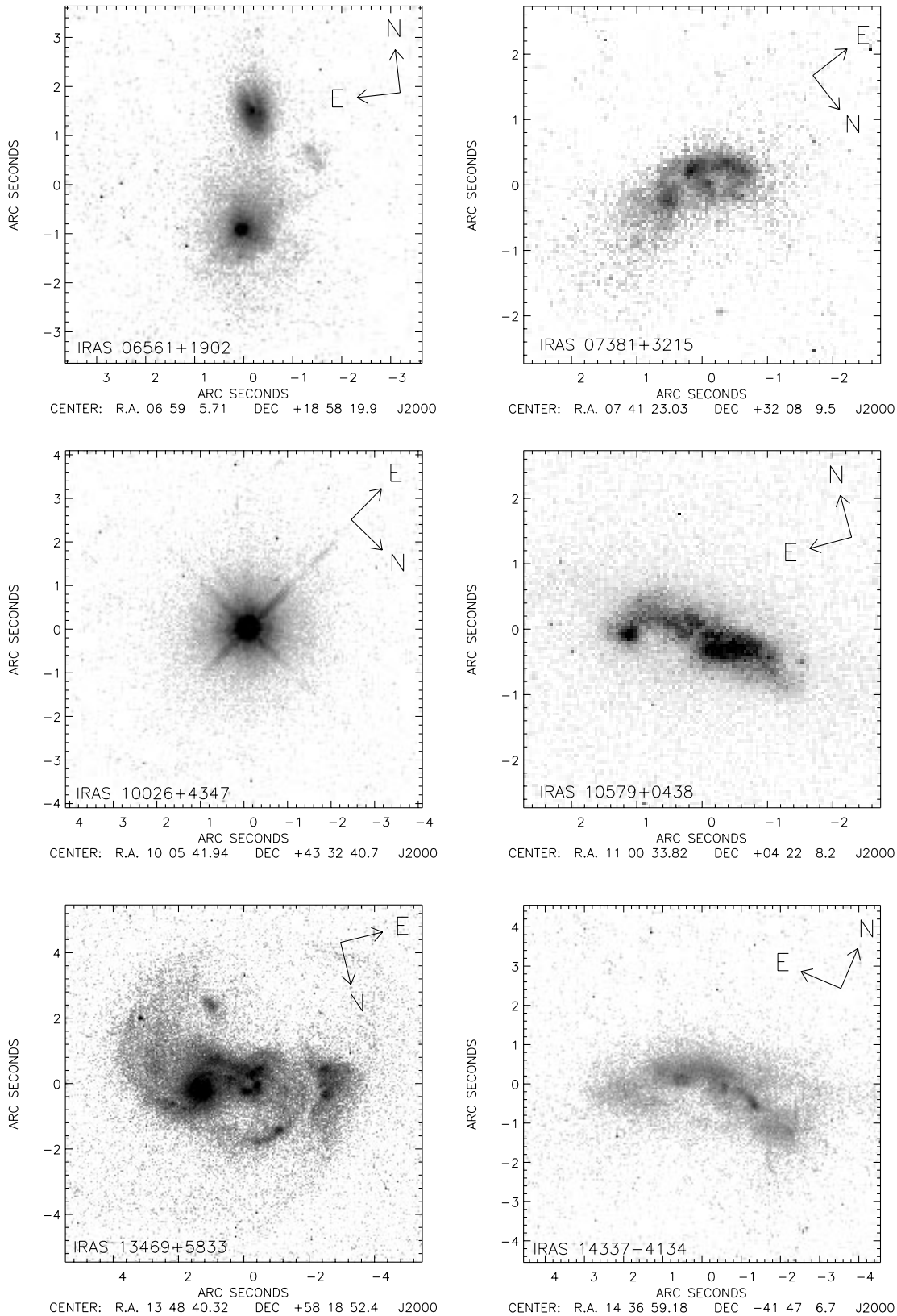

Figure 2. *HST* F606W images of IRAS 06561+1902 to IRAS 14337−4134.

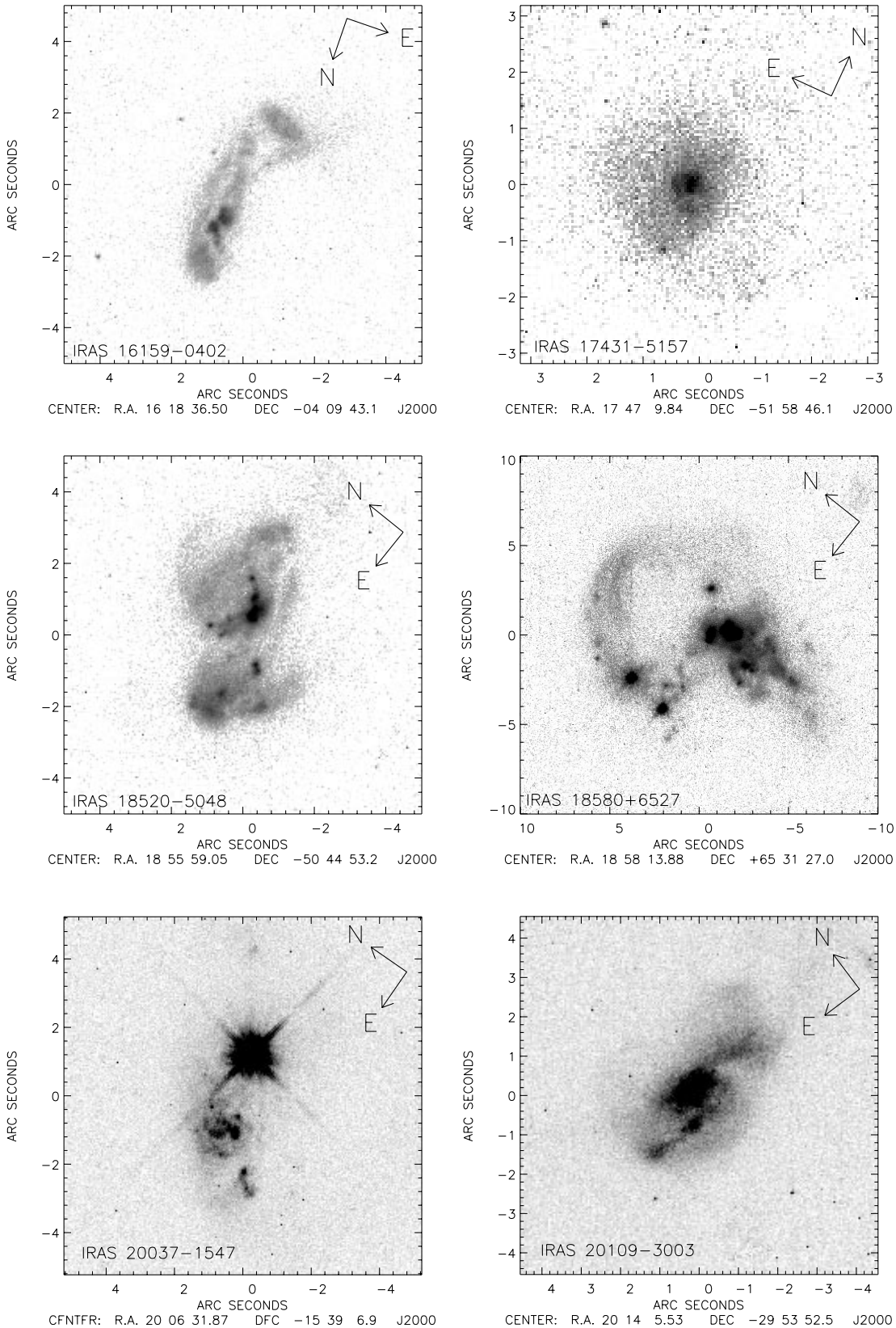

Figure 3. *HST* F606W images of IRAS 16159−0402 to IRAS 20109−3003.

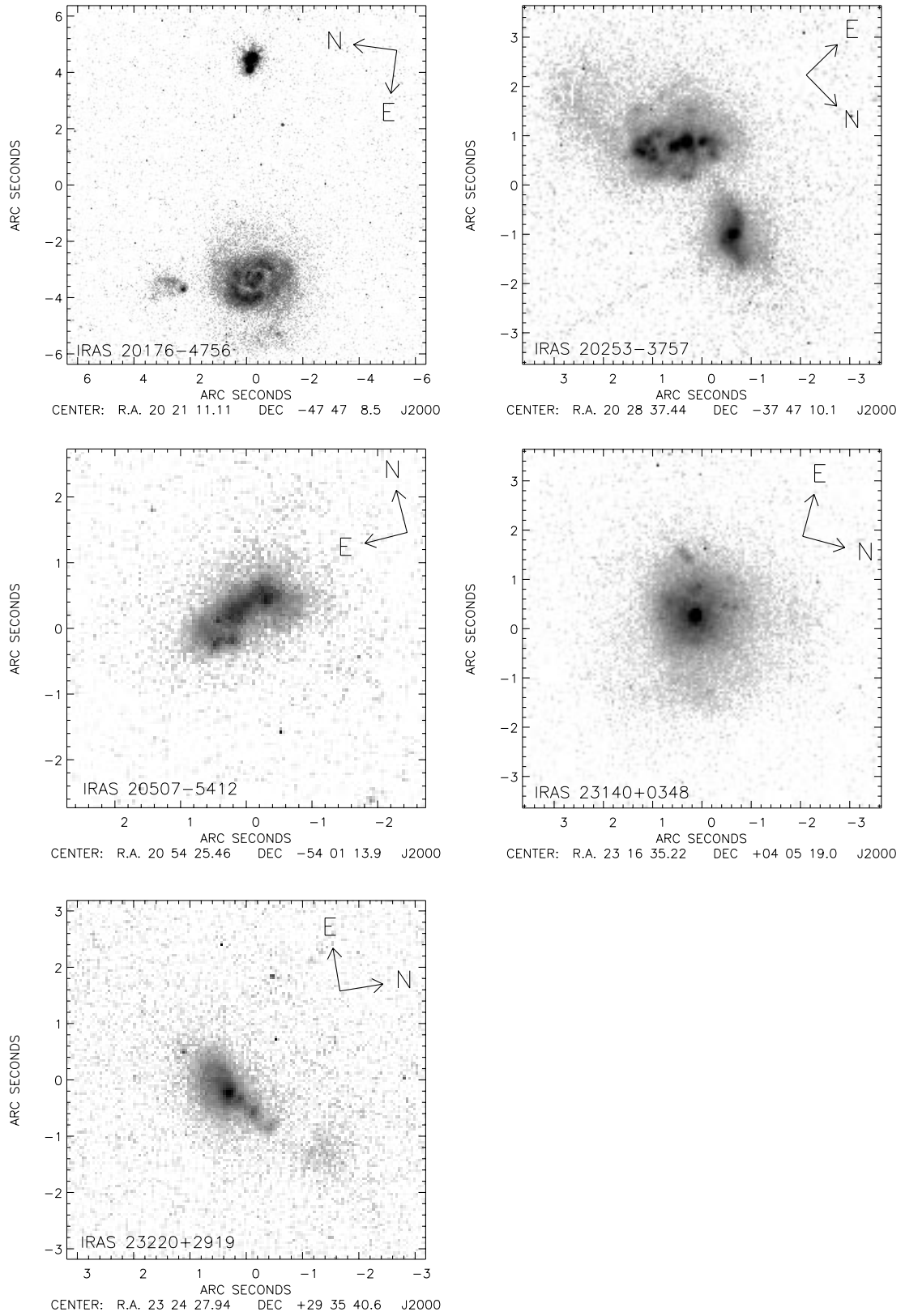

Figure 4. *HST* F606W images of IRAS 20176−4756 to IRAS 23220+2919.

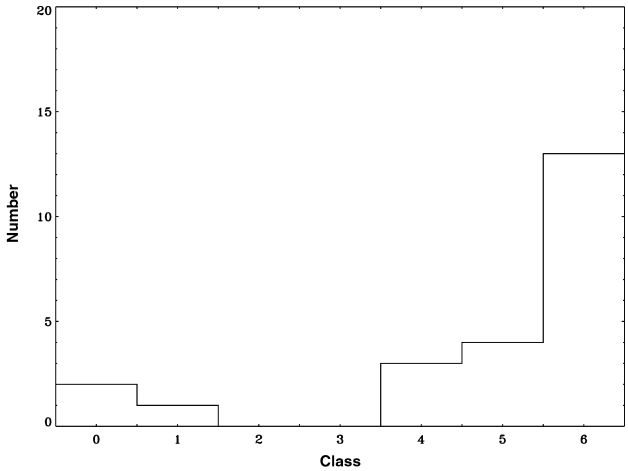

Figure 5. Histogram showing the number of sources per band in the seven band classification system of Lawrence et al. 1989. A summary of this classification scheme can be found in Section 4.1.

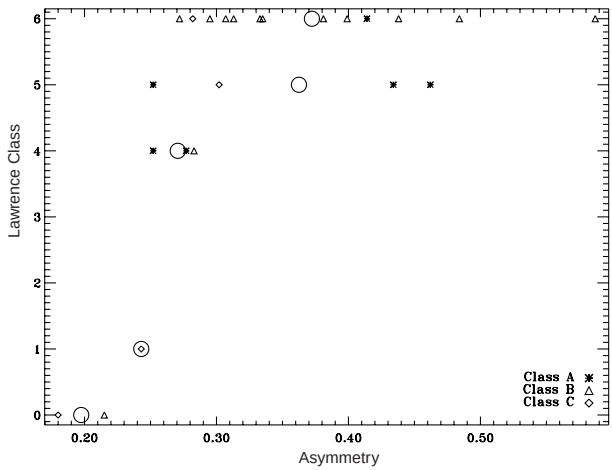

Figure 6. Comparison between the Lawrence et al. classification scheme, the qualitative classification scheme described in Section 4.1 and the asymmetry statistic *A* described in Section 4.1. The three different systems, although based on different criteria, overall give similar descriptions. The three systems are therefore measuring related physical quantities, as expected. The circles denote the mean asymmetry for each Lawrence et al. band.

elliptical galaxy. Using the above classification scheme, 3/23 of the sample are classified as not interacting (groups 0–2), 3/23 of the sample are classified as having a nearby companion but showing no signs of interaction (groups 3–4), and 17/23 are classified as interacting or peculiar (groups 5–6). Fig. 5 shows a histogram of the number of sources in each band. If it is assumed that the three sources with a nearby companion are interacting then this gives a fraction of ULIRGs observed to be interacting of 87 per cent. If it is assumed that the sources with a nearby companion are not interacting then this gives a minimum observed interacting fraction of 74 per cent.

For some purposes it is informative to classify the ULIRGs into broader categories based solely on qualitative descriptions of their optical morphology. We have therefore classified our sample as follows.

Class A: There are two separate sources, but they are close enough to assume reasonably that they are interacting, or they are interacting but still physically distinguishable as separate objects.

Class B: The source is not distinguishable into separate objects and there is no QSO activity, but there are clear signs of interaction such as tails, bridges and multiple nuclei.

Class C: The source contains an optical QSO with or without signs of ongoing interaction.

These classes are chosen such that sources can be classified unambiguously. They are not intended to imply an evolutionary sequence. By these criteria, five sources are identified as class A, 14 as class B and four as class C. The classification of individual objects is given in Table 1. Analysis using this qualitative classification scheme is given in Section 5.

A quantified estimate of the degree of disturbance in an object can be obtained by computing some form of asymmetry statistic. Numerous different methods exist, a popular approach is to compute the 180° statistic *A*. Here we use a modified form of the equation presented in Brinchmann et al. (1998) and used by e.g. Serjeant et al. (2000):

$$A = \frac{\sum_{ij} |I_{ij} - I_{ij}^T|}{2\sum_{ij} |I_{ij}|} - k \qquad (4)$$

where I_{ij} is the original image, I_{ij}^T is the image following a 180° rotation, and k is the sky asymmetry statistic:

$$k = \frac{\sum_{ij} |G_{ij} - G_{ij}^T|}{2\sum_{ij} |G_{ij}|} \qquad (5)$$

where G_{ij} and G_{ij}^T are areas of sky equal in area to the object image. There are two differences between the formula used by Brinchmann et al. and our formula. The extra factor of 2 in both equations ensures that the asymmetry statistic is normalized to between 0 (perfect 180° symmetry) and 1 (perfect 180° antisymmetry). The modulus on the denominator ensures that sky values are not overestimated. For the QSOs in the sample the asymmetries are computed for the host galaxies rather than for the QSOs themselves as the QSOs will otherwise dominate and lead to unrealistically low values. For each object the asymmetry was calculated for all possible positions within the object and the lowest value was then selected. The computed asymmetry values can be found in Table 1.

A comparison between the Lawrence et al. classification scheme, the qualitative classification scheme described above, and the computed asymmetries can be found in Fig. 6. It is apparent that, despite the different criteria used in these three systems to classify the objects in the sample, the asymmetry statistic *A* gives similar results to both of the more qualitative classification schemes. The three different statistical measures are therefore measuring related physical quantities, as expected.

With the enhanced resolution of *HST* it is informative to examine the morphology of the sample in more detail. Two of the samples (IRAS 02054+0835 and 10026+4347) are QSOs that show no apparent signs of interaction. Two objects (IRAS 00275−2859 and 20037−1547) are mergers containing QSO activity. Three sources (IRAS 06268+3509, 18520−5048 and 20253−3757) are merging galaxy pairs. One source (IRAS 06361−6217) resembles a collisional ring galaxy. 13/23 sources show evidence for tidal tails, plumes, and other signs of ongoing interaction. In addition these sources all show at least one, and in most cases several, compact bright regions or 'knots'. Two sources (IRAS 02587−6336 and

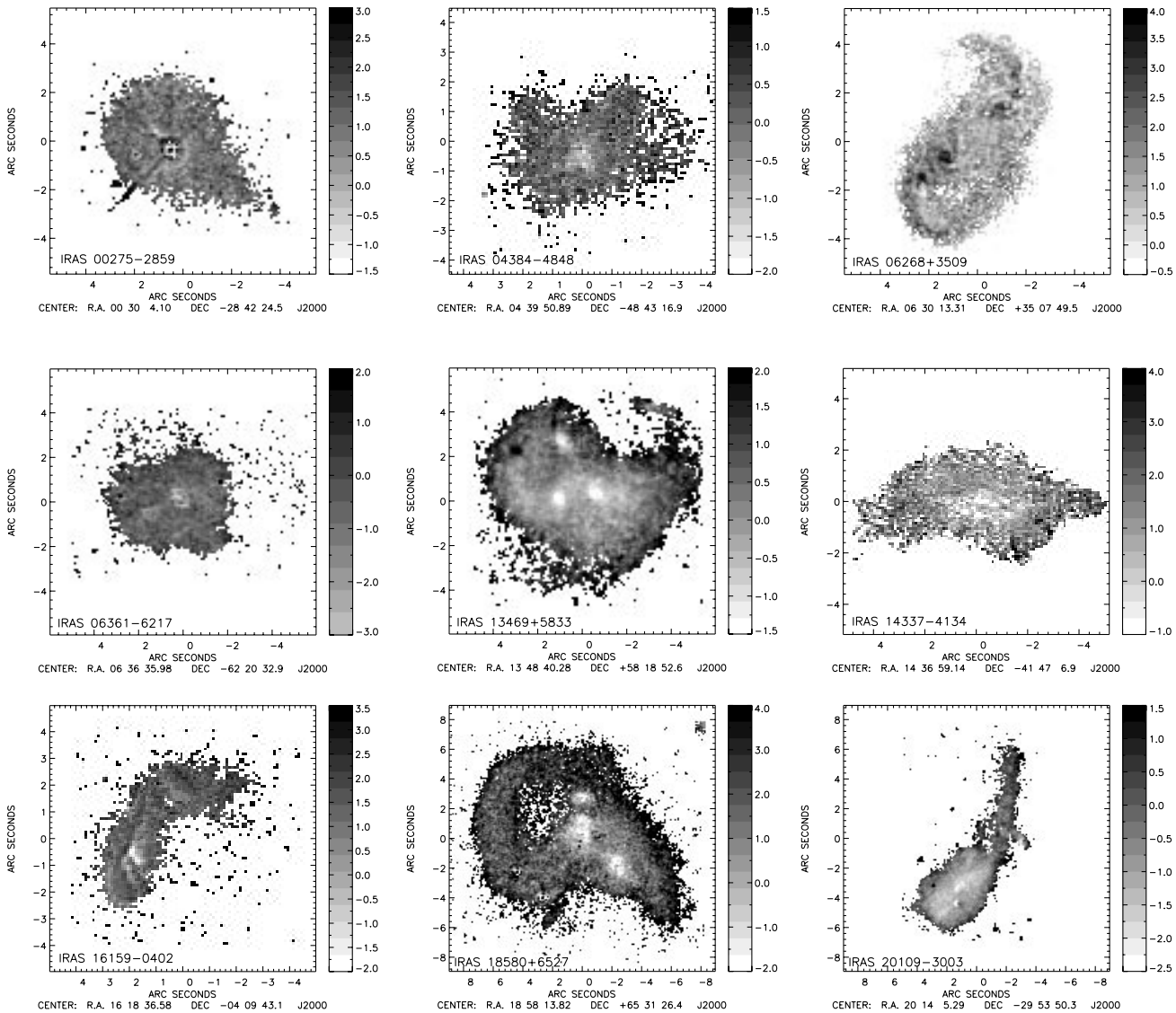

Figure 7. *F*606*W*–*F*814*W* colour maps for nine of the 22 sources. The colourbar gives the range in colour for each source. The orientation of each map is the same as the source image. The F606W band data has been degraded to F814W band resolution. The central region of IRAS 00275−2859 is aberrated due to the very bright central point source.

20176−4756) are binary systems. Discussion of the morphology of individual sources can be found in Section 4.4.

Three sources from our sample can be identified as having 'warm' infrared colours ($f_{25}/f_{60} > 0.2$), whereas ten sources have 'cool' infrared colours ($f_{25}/f_{60} < 0.2$). The remaining ten sources have *IRAS* upper limits that do not allow us to distinguish between these two possibilities. Of the three 'warm' sources, two are QSOs, one of which shows signs of interaction. Of the ten 'cool' sources, one is an interacting system containing QSO activity, one is a close pair, and the rest are interacting systems. Two of these interacting systems (IRAS 13469+5833 and 18580+6527) show evidence for a violent merger, with large numbers of bright knots and large tidal tails.

4.2 Colour maps

Colour maps have been constructed for those nine sources that show sufficient spatial extension in both the F606W and F814W band images, and are presented in Fig. 7. Sky background regions, and those regions with low signal-to-noise (S/N), have been masked out. The slightly lower S/N in the F606W band means that excessively reddened (dark) regions with low S/N are masked off. This effect is most apparent in IRAS 18580+6527 and 20109−3003, where the maps become increasingly dark towards the edges of the objects before being masked off.

One object (IRAS 00275−2859) displays a smooth colour structure (discounting the slightly aberrated centre), perhaps indicating the presence of a uniform dust shroud or screen obscuring the central illuminating source. The other colour maps all display evidence for a large-scale non-uniform colour structure which cannot be attributed to artefacts of amplified noise spikes in the deconvolved images. Two objects (IRAS 04384−4848 and 14337−4134) show a central, extended, diffuse blue region. One object (IRAS 06268+3509) shows several red, compact regions coinciding with the centres of the two merging galaxies. We interpret these as heavily obscured star formation regions. The remaining sources show a number of blue or red compact 'knots', in most cases located towards the central regions. The blue regions are most plausibly interpreted as areas of enhanced, unobscured star formation, and the red regions as either dust-shrouded star formation or remnant nuclei from the merger progenitors. Care

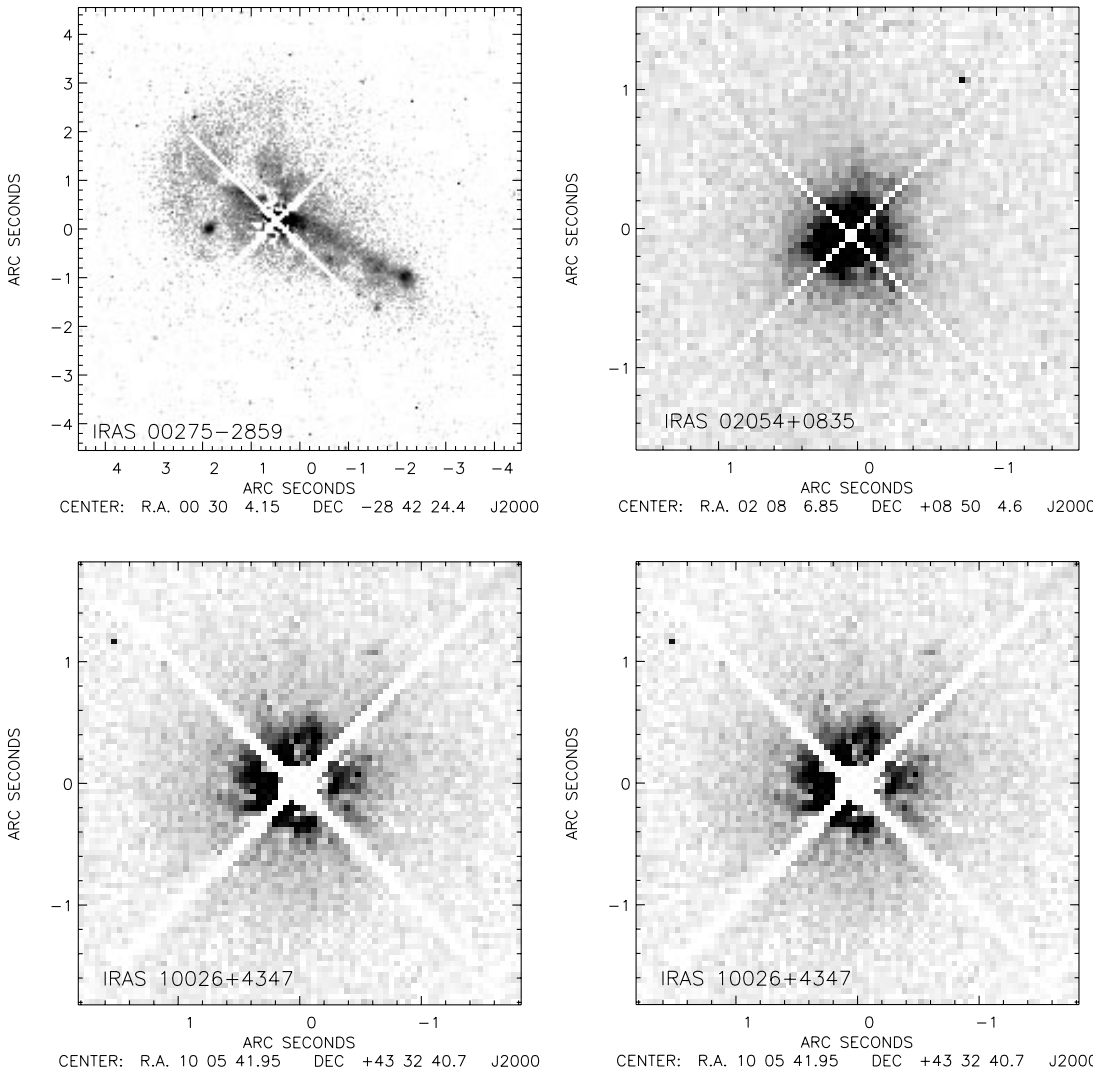

Figure 8. *HST* F606W images of the ULIRG QSO host galaxies. Residual PSF features have been masked out.

Table 3. QSO host galaxy properties.

Source	M_V	r_e (kpc)	I_e	Notes
00275−2859	–	–	–	Interacting
02054+0835	−22.63	3.7	20.7	Elliptical, low ϵ
10026+4347	−21.14	6.6	22.2	Elliptical, disturbed
20037−1547	–	–	–	Interacting

Properties of the host galaxies of the four objects in the sample containing an optical QSO. Data for the two interacting hosts are not given.

must be taken in interpreting such regions from imaging data alone. An alternative interpretation is that these regions are reflected light from an obscured AGN, as observed in Mrk 463 (Uomoto et al. 1993). Although most ULIRGs (≥80 per cent) are starburst dominated, AGN reflected light could still be a potential source of uncertainty in classifying knots as most starburst dominated ULIRGs have a significant AGN component, especially at higher luminosities. Another possibility could be shock fronts from an expanding superwind (Heckman, Armus & Miley 1990). Although a superwind might be expected to produce a systematic colour gradient as opposed to a point-like structure, comparisons between locally observed superwinds (Heckman et al. 1990; Wang et al. 1997) show that, at the mean redshift of our sample, a superwind could create a small structure only a few pixels (∼5) across. A final possibility is that of small holes in locally obscured regions, caused by photodestruction of dust grains by hot young stars. These alternate possibilities are impossible to discount completely without spectroscopic data.

4.3 Host galaxies

Four of the objects in the sample contain some form of optical QSO. Host galaxy images for these four QSOs are presented in Fig. 8. Data for the host galaxies are presented in Table 3.

Host galaxies were clearly detected in all four QSOs. For IRAS 20037−1547 and 00275−2859 both spiral and elliptical light profiles were very poor fits to the underlying light distribution and the host galaxies are clearly interacting. For IRAS 02054+0835 and 10026+4347, the host galaxies were well fitted by an elliptical profile ($\chi^2 \sim 1.4$), with a spiral profile being a much poorer fit

to the data ($\chi^2 \sim 4.0$). We investigated the possibility that we were merely fitting the bulges of spiral host galaxies by fitting simultaneously elliptical and spiral components in the central and outer regions, respectively, the radius of each component being allowed to vary. In both cases it was found that a 'pure' elliptical profile was strongly preferred.

IRAS 02054+0835 has a host galaxy which displays no evidence for ongoing interactions. The ellipticity is low ($\epsilon \sim 0.05$) and there is no isophotal twisting. The other resolved host galaxy (IRAS 10026+4347), although well fitted by an elliptical profile, also shows moderate disturbance. Although having only two resolved hosts means comparisons with other samples are necessarily limited, our host galaxy properties are similar to early-type galaxies in the Fornax and Virgo clusters (Caon, Capaccioli & D'Onofrio 1994), and to elliptical galaxies at higher redshifts (Kelson et al. 2000).

Of the remaining 19 objects in the sample without an optical QSO, 17 are too disturbed to attempt fitting any form of galaxy profile. The remaining two objects (IRAS 17431−5157 and 23140+0348) have a sufficiently regular morphology such that it might be expected that fitting galaxy profiles would yield informative results. Although one profile was clearly preferred in each case it was not possible to obtain a 'good' fit for any profile. Reduced χ^2 values were of the order 3 for the best fit in each case. We therefore conclude that these galaxies, despite being regular in appearance, have a light profile not consistent with a dynamically relaxed spiral or elliptical galaxy and are therefore disturbed.

4.4 Individual sources

In the following descriptions, comments regarding *HST* images refer to the F606W PC images.

IRAS 00275−2859: This IR luminous QSO was discovered by Vader & Simon (1987). Clements et al. (1996b) calculate a dust temperature of 54 K and a dust mass of $7.3 \times 10^7\,M_\odot$ for this object, assuming a linear emissivity–frequency relation and a monolithic dust population whose temperature is solely defined by the 60/100-μm flux ratio. Zhenlong et al. (1991) classify this object as having a near (<10 arcsec) faint companion but not interacting. Clements et al. (1996a) classify this object as 'disturbed'. The *HST* image shows strong interactions and a double nucleus. The north-eastern nucleus contains a QSO. There is also a spatially (but not luminally) symmetric halo extending about 2 arcsec. There is one very bright 'knot' near the QSO, and a number of dimmer knots near the south-western nucleus. Canalizo & Stockton (2001) classify this second nucleus as a giant H II region rather than an AGN. The faint companion described by Zhenlong et al. is revealed to be an undisturbed spiral.

IRAS 02054+0835: A QSO with no signs of ongoing interaction. There are, however, five small, faint sources within 10 arcsec.

IRAS 02587−6336: Previous optical imaging (Zhenlong et al. 1991) classified this system as a close pair with interaction. The *HST* image shows a binary system. Both sources show signs of disturbance, although there are no tails or loops and the sources appear still physically separate. The brightest source is a disturbed spiral, with a smaller source to the south-west.

IRAS 04384−4848: A small, disturbed source with no QSO activity. There are a number of compact bright regions and two faint tails.

IRAS 06268+3509: A pair of merging spirals. The northern spiral contains several compact bright 'knots'. There are four further small sources within 12 arcsec.

IRAS 06361−6217: Zhenlong et al. (1991) classify this object as being non-interacting, but with a nearby companion. The *HST* image shows a source with a collisional ring galaxy morphology. The south-eastern nucleus is very bright, with several nearby knots. A faint, elliptical halo surrounds these regions, with a semimajor axis length of about 8 arcsec. The western region is smaller and dimmer, with no bright knots. There is a small, faint companion 10 arcsec to the north, and an object 15 arcsec to the south which is either a QSO or a foreground star.

IRAS 06561+1902: An interacting pair with a close companion. Although still physically distinct, the two interacting galaxies are connected by a faint bridge of nebulosity. This source is striking in that there is a similar group of three objects 10 arcsec to the south-west, one of which is a QSO.

IRAS 07381+3215: A small, peculiar galaxy with some bright star-forming regions. Notable are the two foreground stars 15 arcsec south-east of the source.

IRAS 10026+4347: This object shows less than 1 per cent polarization in the optical/UV, rapid X-ray variability and no optical absorption, indicative of a low quantity of dusty gas in the object and zero intrinsic polarization, and probably indicative of a direct, unobscured line of sight to an AGN disc or nucleus (Grupe et al. 1998). The optical and X-ray properties of this object are discussed extensively by Xia et al. (1999), who describe the source as a post-merger system with strong Fe II emission. It shows a steep X-ray continuum slope, an X-ray luminosity comparable to that of Sy1s or QSOs, large rapid X-ray variability, and optical continuum variability. The intense Fe II emission is cited as being the result of gas enrichment by supernovae. The *HST* image shows a QSO with no apparent signs of interaction. There are three very faint sources within 12 arcsec.

IRAS 10579+0438: The *HST* image reveals a small source with two bright regions separated by about 1.5 arcsec, linked by a small tail. The western region is brighter, larger and more disturbed than the eastern region. The only object within 30 arcsec is a foreground star.

IRAS 13469+5833: Ground based optical imaging (Leech et al. 1994) showed an interacting system with giant tails. The *HST* image shows a large and complex morphology. There is a large, bright, circular region to the west with a radius of approximately 1 arcsec. To the east of this there is a cluster of smaller 'knotlike' regions. There are two large tails on the east and west sides of the source. Large numbers of bright 'knots' are also apparent throughout the source. There are two faint sources 15 arcsec to the west.

IRAS 14337−4134: Zhenlong et al. (1991) identify this source as a close pair with a tidal tail, and classify it as interacting. The *HST* image shows a merging system with several bright regions and two small tidal tails. There are four bright sources within 25 arcsec.

IRAS 16159−0402: This interacting source shows a bright, peanut-shaped region with some small knots immediately to the north. Further north there is a larger, dimmer region. A tail or plume stretches south to an inclined disclike structure.

IRAS 17431−5157: A bright, disturbed core surrounded by a dim asymmetric halo. There are a large number of other sources within the PC field of view.

IRAS 18520−5048: Zhenlong et al. (1991) describe this object as being non-interacting but having a close faint companion. Clements & Baker (1996) however argue that this system in fact possesses two nuclei separated by 2.5 arcsec. The *HST* image

reveals an interacting pair of spirals. The two spirals are similar in size and brightness, both having a number of small, bright 'knots'.

IRAS 18580+6527: This source is cited as a possible multiple nucleus ULIRG (Auriere et al. 1996). Leech et al. (1994) tentatively identify this source as a merger system interacting with a companion. The western source has a Sy2 spectrum and the eastern source has an H II spectrum. The *HST* image shows a source that is strongly interacting. There is a large, bright region to the west of the source, with several smaller bright regions surrounding it. To the east there are two smaller bright regions, together with a very large tail extending approximately 10 arcsec to the north-west. The western region appears brighter and more active than the eastern region.

IRAS 20037−1547: An interacting system containing a QSO. Remnants of one of the merger progenitors lie to the east. Physical merging appears to have only just started in this system.

IRAS 20109−3003: A pair of merging spirals. There are two compact, bright regions separated by about 1 arcsec, which can plausibly be identified as the galaxy nuclei. The north-western region is both larger and brighter than its south-western counterpart. A long 'tail' extends about 10 arcsec to the west, and there are no companion sources.

IRAS 20176−4756: This source is difficult to interpret. The most plausible picture is a binary system consisting of a very compact double nucleus source and a slightly disturbed spiral with a small companion, separated by 30 kpc. Under this interpretation, this source would be in the earliest stages of interaction. It is however not possible to draw solid conclusions without redshifts for both sources. The quoted redshift is for the spiral.

IRAS 20253−3757: An interacting pair with no nearby companions. The northern galaxy is a disturbed spiral, with arms extending to the north and south. A number of luminous 'knots' are apparent in the southern galaxy, extending east–west.

IRAS 20507−5412: This source is small, luminous and displays a number of compact bright regions. There are two bright sources within 15 arcsec, to the south-east is a spiral and to the north-east is a small QSO.

IRAS 23140+0348: Yee & Oke (1978) reported broad wings on both Hα and Hβ for this radio-loud source. An optical polarisation study (Draper, Scarrott & Tadhunter 1993) reveals two polarization components, one intrinsic to the nucleus and the other restricted to elongated or 'fan-like' areas. This implies that significant amounts of radiation are escaping at large angles to the radio axis. The core is described as having a compact steep radio spectrum with extensions to the east and west. The optical spectrum of the associated galaxy is characteristic of young A-type stars. An intensity contour map of the source shows circular isophotes, whereas polarized intensity isophotes are very anisotropic, showing a 'fan' to the south-west and a slight enhancement to the north-east. The radio axis of the source does not coincide with any of the polarization axes of the source. The flux from the radio core of this object is uncertain. Early studies (Ulvestad 1985) do not agree with later very large array (VLA) studies (Harvanek & Hardcastle 1998). Heckman et al. (1994) identify this source as a narrow line radio galaxy. Interestingly, this source is a member of one of the 'compact groups' identified by Hickson (1982), these groups being characterized as possessing at least three members, having a high density and a low velocity dispersion. Members of such groups would therefore undergo almost continuous gravitational perturbation and could be candidate sites for triggering ULIRG activity (Borne et al. 2000). The *HST* image shows a bright source with small, dim knots to the east and north. There is a dim asymmetric halo, extending towards the north-west.

IRAS 23220+2919: A small source with a bright nucleus to the south-east and an extension to the south-west which probably contains a second smaller, dimmer nucleus. There are no companion sources within a 15 arcsec radius.

5 DISCUSSION

5.1 Sample morphology

The large-scale morphology of ULIRGs has been studied by many authors, often with conflicting results. Sanders et al. (1988) found that 100 per cent of a sample of 10 ULIRGs showed signs of interaction. Lawrence et al. (1989) found that, although 19/41 *IRAS* galaxies with $L_{60} > 10^{11}\,L_{\odot}$ were interacting (where L_{60} is the 60-μm luminosity computed from the *IRAS* 60-μm flux), only 2/6 *IRAS* galaxies with $L_{60} > 10^{12}\,L_{\odot}$ were interacting. Near IR imaging of a sample of nine ULIRGs (Carico et al. 1990) showed that four of the sample possessed double nuclei with high activity levels, and they estimated the mean starburst lifetime to be 4×10^8 yr. VLA observations of two complete samples of ULIRGs (Sopp, Alexander & Riley 1990) found several binary starbursts, and that starburst activity can be triggered in both, either or neither galaxy in an interacting pair. Zhenlong et al. (1991) derived an interacting fraction of 61 per cent for their sample of 41 ULIRGs. Leech et al. (1994) imaged 35 ULIRGs and found that 23/35 showed signs of interaction. Their results also revised the interaction fraction quoted by Lawrence et al. (1989) from 2/6 to 4/6. Clements et al. (1996a) derived an interacting fraction of 90 per cent for their sample of 60 ULIRGs. They explain the discrepancy between their results and previous work by saying that deep optical imaging is needed to detect faint signs of interactions and that previous studies may have missed such signs. Observations of the *IRAS* 1Jy sample of ULIRGs (Kim & Sanders 1998) found a luminosity function of the form $\Phi(L) \propto L^{-2.35}$, strong density evolution with $\alpha = 7.6 \pm 3.2$, and no evidence for clustering. Murphy et al. (1996), using optical and near-IR imaging of a sample of 56 ULIRGs, quote 95 per cent as involved in current or recent interactions. Surace et al. (1998) performed deep *B*- and *I*-band imaging using *HST* for a sample of nine 'warm' ULIRGs and found that all showed signs of ongoing interactions. They also found that most of their sample contained a number of compact blue 'knots' of star formation that do not contribute significantly to the bolometric emission, and that a small number of these knots were plausibly active nuclei. Overall they found that their results were consistent with 'warm' ULIRGs representing a critical transition phase between a galaxy merger and a QSO. A complementary study of a sample of 'cool' ULIRGs (Surace, Sanders & Evans 2000) found that all of the sample were either advanced mergers, or early stage mergers with evidence for separate (> 600 pc) nuclei. Emission from the central regions was, with one exception, consistent with high rates of star formation. Murphy et al. (2001), using integral field spectroscopy of a sample of four ULIRGs, propose that the ULIRG phase may be bimodal in time with some ULIRGs being early stage mergers and some being late stage mergers. They further propose that multiple starburst events may take place during the ULIRG phase and that some LIRGs may be 'resting' ULIRGs.

The number of sources observed to be interacting in our sample of ULIRGs is 87 per cent, with a lower bound of 74 per cent. These results are in excellent agreement with the more recent ULIRG morphology studies using deep, high-resolution ground- and space-based imaging, although care must be taken in comparing

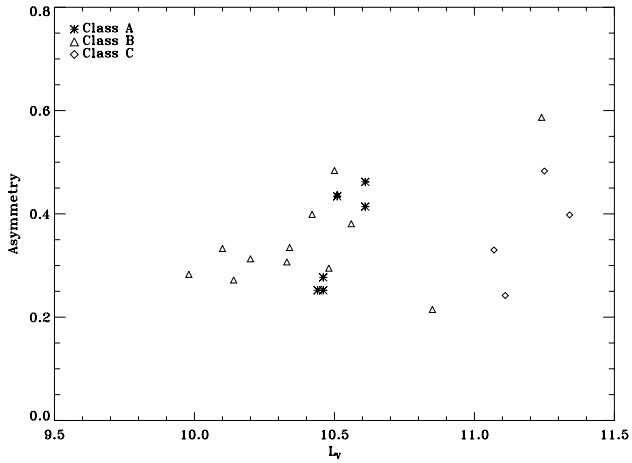

Figure 9. Luminosity in the V band, L_V, versus asymmetry factor (after subtraction of QSO in case of sources shown in Fig. 8). The different symbols correspond to the classification of section 4.1 (class A – two separate sources; class B – interacting galaxies; class C – QSO).

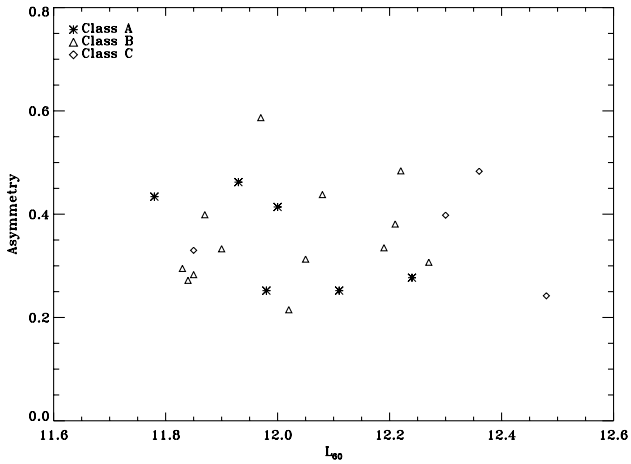

Figure 10. 60-μm luminosity plotted against asymmetry for all 23 ULIRGs. Description of the classes A, B and C can be found in Section 4.1.

this fraction to lower resolution samples. Five of the sources are binary systems where the progenitors have yet to coalesce. The merging systems show a wide range of morphological features and asymmetries, most containing at least one compact luminous 'knot'. Of the four QSOs two (IRAS 02054+0835 and 10026+4347) show no signs of recent interaction. The other two QSOs are still interacting. In one case (IRAS 00275−2859) the merger is advanced, whereas in the other (IRAS 20037−1547) the QSO and galaxy have only just started to merge physically.

The Sanders et al. picture of ULIRG evolution (Sanders et al. 1988) postulates that ULIRGs are the dust-shrouded precursors to optically selected QSOs. According to this picture (hereafter referred to as the S88 picture), interactions and mergers between gas rich spirals transport gas to the central regions of the galaxies. This large central gas concentration triggers starburst activity, and in the latter stages of the merger creates or commences the fuelling of a central active supermassive black hole. This central black hole rapidly comes to dominate the IR luminosity of the ULIRG. In the last stages the dust screen shrouding the black hole is blown away and the ULIRG evolves into an optical QSO.

The sample presented here provides excellent evidence that ULIRGs are strongly linked with both galaxy interactions and (to a lesser extent) QSO activity. That QSO activity is physically connected with ULIRGs is clearly demonstrated by the number of optical QSOs in the sample. If the two phenomena were unconnected then the number of objects in the comoving volume out to $z = 0.4$ which are by chance both ULIRGs and QSOs is 0.1 (Canalizo & Stockton 2001). The sample includes still physically separate but interacting spirals, violent mergers with large amounts of associated star formation, QSOs with signs of ongoing interaction, and QSOs with no apparent signs of interaction. Those sources that are classified as isolated and non-interacting according to the system of Lawrence et al. are all QSOs.

Looking solely at the optical morphologies of the sample it is, however, far from clear that the S88 picture describes the sample well. It is not possible to rule out from this data alone that, for the two QSOs with no signs of ongoing interaction, the IR emission was not triggered by interactions, a counterpart of which exists for the HLIRG population as well (Farrah et al. 2001). In two sources, a QSO is coeval with galaxy interactions. If it is assumed that the e-folding time-scale of an Eddington luminosity black hole with accretion efficiency $\epsilon = 0.1$ is a good estimate for the lifetime of a QSO (Rees 1984) then it is entirely plausible that for these two sources the QSO will burn out before the merger is completed and the system is dynamically relaxed. A straightforward interpretation of all ULIRGs as being a transition stage between galaxy mergers and QSOs is not supported by this data.

Previous studies have also highlighted potential problems with the S88 picture. Mid-IR spectroscopy of 62 ULIRGs (Rigopoulou et al. 1999) found that the majority were powered by starbursts, and that most did not contain a buried QSO. There was no evidence that advanced mergers are more AGN-like, based on the ULIRG nuclear separations. That AGN activity becomes more prevalent with merger advancement is a natural prediction of the S88 picture. A mid-IR spectroscopic survey of 15 ULIRGs (Genzel et al. 1998) found that ∼ 80 per cent were powered predominantly by starbursts and that ∼ 20 per cent were powered by AGN, although at least half the sample showed clear evidence for both types of activity. There was no detected trend for the AGN-like systems to reside in the more compact (and hence more advanced merger) systems. Canalizo & Stockton (2001), in a study of a sample of nine QSOs with far-infrared (FIR) colours intermediate between ULIRGs and QSOs, proposed a model in which some ULIRGs evolve to become classical QSOs in a short time (≤ 300 Myr) and that some QSOs are born under the same conditions as ULIRGs but with a very short (≤ 300 Myr) lifetime. They further propose that the QSO nuclear regions are initially shrouded in a dust cocoon, an idea qualitatively similar to the S88 picture.

Our data do not allow us to discriminate between IR emission due to starbursts and that due to AGN activity. We can, however, examine this topic in alternative ways. If the IR luminosities of the ULIRGs with a QSO are compared with the IR luminosities of the ULIRGs without a QSO via a Kolmogorov–Smirnov (K–S) test, the probability P that the IR luminosities of these two populations are drawn from the same distribution is found to be $P = 0.0411$. Thus it seems very likely that there is a difference in the distributions of the IR emission between those sources with a QSO and those without a QSO (as also found by numerous previous studies), consistent with some form of evolution between a starburst and AGN phase. A plot of L_V versus asymmetry statistic A (equation 4) can be found in Fig. 9. The sources that contain a QSO have comparable asymmetries to the non-QSOs in the sample, with $\langle A \rangle = 0.36$ for the QSOs as opposed to $\langle A \rangle = 0.35$ for the non-QSOs. This suggests that QSOs (and hence AGN) are not found in

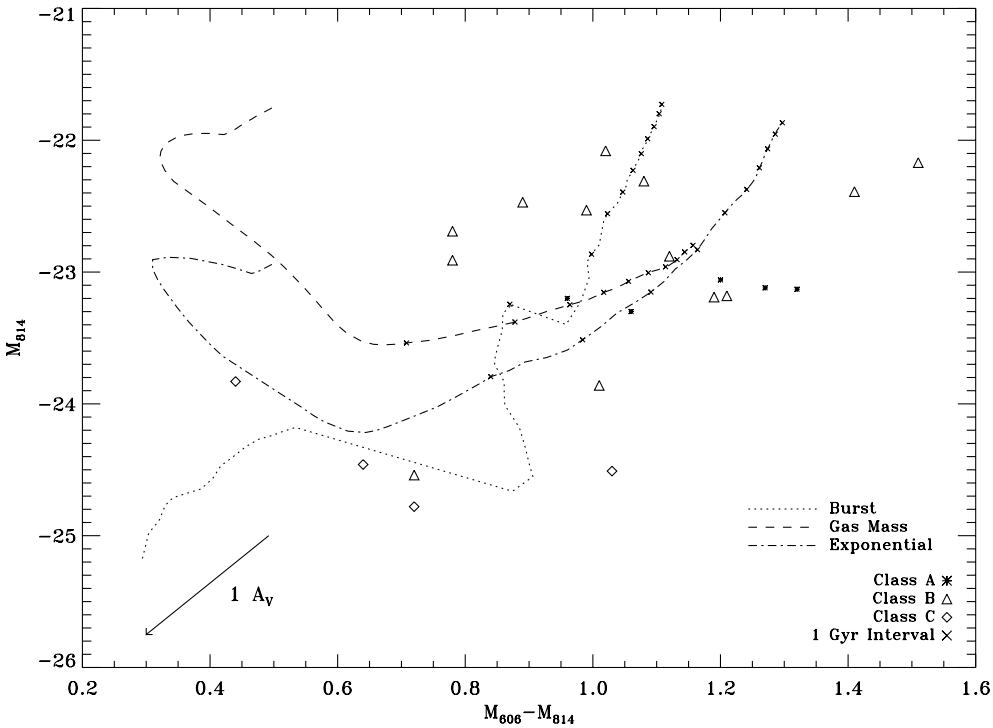

Figure 11. Colour–magnitude diagram for the QDOT ULIRGs. Evolutionary tracks are for a Salpeter IMF and run from 10 Myr to 10 Gyr. The dereddening vector is shown in the bottom left. Time direction for the tracks is L–R. 'Burst' – instantaneous burst of star formation at $t = 0$. 'Exponential' – star formation law of the form SFR $= e^{(-t/1000)}/1000$. 'Gas mass' – SFR $= M_{gas}/3000$. The class C points are not QSO subtracted, and are plotted for comparison only.

more advanced mergers, a result in direct contradiction of the S88 picture and indirectly supportive of Rigopoulou et al. (1999). A plot of L_{60} versus A can be found in Fig. 10. Amongst those sources with no QSO there is no correlation between asymmetry and IR luminosity. Both class A and class B objects are found across a wide range of IR luminosities with no apparent trends. There is some support for the idea that ULIRGs become more AGN-like at the highest IR luminosities (Veilleux et al. 1995; Shier, Rieke & Rieke 1996) as three of the four most IR luminous objects in the sample are QSOs.

We performed simulations to assess the impact of both large-scale features such as tidal tails, and small-scale features such as star-forming knots, on our derived asymmetry values. It was found that, although both large- and small-scale features contributed to the derived asymmetry values, the asymmetries were determined predominantly by the large-scale morphologies. The asymmetry values are therefore an accurate measure of the degree of disturbance in our sample, rather than solely a measure of the number of star-forming knots or other small-scale structures.

Unfortunately there are no other galaxy samples for which direct comparisons between asymmetry values can be made. The closest samples available are the optical starburst sample of Brinchmann et al. (1998) and the subultraluminous radio selected starbursts of Serjeant et al. (2000), both of which lie in a similar redshift range, and were imaged with the PC on *HST* but using the F814W filter. Although the difference in filters means that different stellar populations are being sampled, the closeness in wavelength between the F606W and F814W filters means that this difference should not significantly affect large-scale morphologies. After accounting for the extra factor of 2 in our version of the asymmetry statistic, our computed values are very similar to those computed by Serjeant et al. (2000), with a slightly higher mean value. They are much higher than those values presented by Brinchmann et al. (1998). This implies increasing asymmetry with increasing star formation rate (SFR).

The images presented here have demonstrated the efficacy of *HST* for detecting signs of interaction where lower resolution ground based images either have shown no signs of interaction or have shown ambiguous results. Three sources (IRAS 00275−2859, 06361−6217 and 18520−5048) have, using ground based imaging, been classified as non-interacting or ambiguous. The very high-resolution *HST* images of these sources have however shown clear signs of interaction, implying that ground based surveys of ULIRGs may underestimate the interacting fraction by 15 per cent or more.

Studies of samples of 'warm' and 'cool' ULIRGs have, quite recently, become active areas of research. *HST* imaging of a sample of warm ULIRGs (Surace et al. 1998) revealed that all the sources lay in advanced merger systems. Imaging of a complementary sample of cool ULIRGs (Surace, Sanders & Evans 2000) revealed that all of the sample were either advanced mergers or 'premergers' where the galaxies were still separate. It has been suggested that warm ULIRGs may represent an important transition stage between cool ULIRGs and QSOs. Two of the three sources in our sample with warm colours are QSOs, consistent with warm ULIRGs containing a higher fraction of QSOs than cool ULIRGs. The cool sample however contains one QSO with ongoing interactions. The mean asymmetry for the warm ULIRGs in our sample is 0.404, whereas the mean asymmetry for the cool ULIRGs is lower, at 0.376. Although our sample supports QSO activity being more prevalent in warm ULIRGs than in cool ones, our data do not support the hypothesis that warm ULIRGs are more advanced mergers than cool ULIRGs.

Comparison between the colour maps and the F606W band

images shows that, in most cases, bright regions in the F606W band images correspond with very blue or very red regions in the colour maps. For three objects however (IRAS 13469+5833, IRAS 04384−4848 and 14337−4134) this is not the case. These objects show blue regions that do not coincide with bright regions in the F606W band images or the F814W band images. As these regions are located towards the centres of the sources, this result can be interpreted as a generally slightly higher SFR, a local underdensity of dust, or a local initial mass function (IMF) skewed towards high-mass stars in what are probably the most turbulent and gas rich regions of ULIRGs. These optically bluer regions may also therefore correspond to sites of buried starbursts and/or AGN.

5.2 Host galaxies

Previous surveys of QSOs using *HST* have generally been extremely successful in detecting host galaxies. Urry et al. (1999) give results for a sample of BL Lacertae objects, detecting host galaxies to a redshift of $z = 0.7$. They find that the hosts are all extremely luminous ellipticals with $\langle M_I \rangle = -24.6$. The derived ellipticities are generally low and morphologies are smooth. Imaging of a sample of 14 quasars (six radio-loud, five radio-quiet, three radio-quiet ultraluminous infrared quasars) by Boyce et al. (1998) showed that all the radio-loud quasars had elliptical hosts, the radio-quiet quasars possessed both elliptical and spiral hosts, and that the radio quiet ultraluminous infrared quasars lay in violently interacting systems. Host galaxies were on average 0.8 mag brighter than L^*. Results from imaging of two luminous radio-quiet quasars (Bahcall, Kirhakos & Schneider 1996) show that both quasars reside in apparently normal host galaxies, one being an elliptical and the other a spiral. Disney et al. (1995) present *HST* imaging for a sample of four QSOs, finding that all four have elliptical hosts. Although they find that the morphologies of the hosts are all featureless, they argue that the presence of multiple very close companions is evidence for interactions as the trigger for the quasar activity.

We resolved host galaxy morphologies in only two of the four QSOs in the sample, finding one to be a smooth elliptical and the other to be an elliptical with signs of disturbance. The hosts of the other two sources were detected at > 99 per cent confidence but it proved impossible to fit an elliptical or spiral profile to the underlying light distributions. The PSF subtracted images show these hosts to be interacting. Although discussion based on only four sources can only be very limited, these results do not contradict the S88 picture, and are also supportive of a link between merging spirals and emerging ellipticals.

5.3 Optical colours

A colour−magnitude diagram (M_{606}–M_{814} versus M_{814}) is presented in Fig. 11. The average F814W band magnitude of those sources which do not contain a QSO is $M_{814} = -22.9$. This is 0.3 mag less bright than the field elliptical galaxy magnitude in the Cousins I band, $M_I^* = -23.2$ (Efstathiou, Ellis & Peterson 1988; Pozzetti, Bruzual & Zamorani 1996;). Still physically separate but interacting systems (class A) have a similar optical magnitude to those systems that are physically merging (class B), with the class A objects having an average magnitude of $M_{814} = -22.93$ and the class B objects having $M_{814} = -22.86$. The QSOs (class C) are much brighter than the field galaxy magnitude, with $M_{814} = -24.4$, and are plotted for comparison only. Similarly, the two objects without an optical QSO but with broad lines (18580+6527 and 23140+0348) are plotted only for comparison.

Evolutionary tracks for three star formation scenarios have been plotted to estimate the contribution of stellar populations of various ages to the optical emission from the class A/B objects. These tracks were computed using the PEGASE package (Fioc & Rocca-Volmerange 1997), suitably modified to produce output in the *HST* flight filter system. An initial mass normalization was selected by assuming that the Milky Way is a suitable template. The total mass of the Milky Way is currently thought to be about $10^{12}\,M_\odot$ (Wilkinson & Evans 1999). A rough estimate for the mass of stars for two merger progenitors (excluding any dark matter component) is therefore about $2 \times 10^{11}\,M_\odot$. Dust extinction effects are included in the models for a spherically symmetric system and are computed individually for each time-step. The calculated optical depth varies between $0 < \tau < 35$.

The $A_V = 1$ dereddening vector, plotted on the lower left of Fig. 11, lies almost parallel to the three evolutionary tracks. Coupled with the uncertainty in the mass normalization, this means that only upper limits can be set on the ages of the stellar populations. Similarly it is not possible to draw conclusions about which star formation scenario is applicable, or to construct more precise constraints on the ages of the stellar populations, as data are only available in two bands which are quite close in wavelength. These limitations considered, the optical emission from nearly all the class A/B ULIRGs is best described by stellar populations of several Gyr or less in age. The most likely interpretation is that the optical emission is dominated by old stellar populations from the merger progenitors, a result consistent with previous studies (Surace et al. 1998), although a heavily dust-shrouded starburst cannot be ruled out.

5.4 Pair mergers versus multiple mergers

The number of objects involved in a typical ultraluminous galaxy merger can have a fundamental impact on both the SFR and (to a lesser extent) the merger morphology. Although the physical mechanisms behind starburst and AGN activity are likely to be no different in pair mergers and in multiple mergers, the fraction of ULIRGs in multiple merger systems can give a good estimate of the fraction of ULIRGs in compact groups of galaxies (Bekki 2001), as mergers between more than two galaxies are expected to occur naturally in compact groups (Barnes 1989; Hickson 1997). Numerical simulations of a merger between five disc galaxies (Bekki 2001) showed that repetitive massive starbursts are characteristic of multiple galaxy mergers, in contrast to pair mergers where only one or two starbursts occur. Multiple galaxy merging has been previously linked to Arp 220 (Diamond et al. 1989). Models for multiple galaxy mergers (Taniguchi & Shioya 1998) propose that the existence of more than two AGN or starburst nuclei is evidence for a multiple merger history. It has been suggested (Borne et al. 2000) that Hickson compact groups, where multiple mergers may be expected to take place, may be the progenitors of ULIRGs. It has also been suggested (Murphy et al. 2001) that multiple starbursts, as may be expected to occur in mergers between more than two galaxies, may be common in ULIRGs.

For those objects in our sample where the progenitor galaxies are no longer distinct (class B/C) it is difficult to draw reliable conclusions about the number of merger progenitors, as the complex geometries of gas and dust in these systems can easily give rise to multiple bright regions. Even using optical

spectroscopy to identify separate AGN regions as a method for counting the progenitors could be ambiguous. AGN regions could be heavily obscured by dust making them invisible in the optical. Alternatively some models suggest (Taniguchi, Ikeuchi & Shioya 1999) that an AGN could form in a galaxy merger via the collapse of a star cluster containing compact supernova remnants, without the need for a 'seed' black hole from the merger progenitors. Although we cannot use our data to establish accurate fractions of ULIRGs in pair mergers and multiple mergers, we can examine whether pair merging and multiple merging does in fact take place. For all the ULIRGs in class A the merger appears to be taking place between only two galaxies. This is most apparent in IRAS 06268+3509 and 18520−5048. Conversely, some ULIRGs in the sample (e.g. IRAS 13469+5833 and 18580+6527) show more than two large, well-separated bright regions which cannot plausibly be interpreted as having arisen due to dust obscuration patterns. According to multiple galaxy merger models (Taniguchi & Shioya 1998) this can only arise in mergers between more than two progenitor galaxies. From this, we conclude that ULIRGs can be both pair mergers and multiple mergers, suggesting that ULIRGs can be formed both in compact groups and in isolated pairs.

5.5 ULIRG evolution

5.5.1 Merger, starburst, and ULIRG lifetimes

A *prima facie* picture of how long each stage in a merger is ultraluminous in the IR can be gained from looking at the number of sources in the sample in each merger stage. In five of the sources the galaxies are still physically separate, or they are interacting but still physically distinguishable as separate objects (class A). In 14 sources (class B) separate galaxies are not distinguishable and there are clear signs of ongoing interaction, such as tidal tails, loops, and multiple nuclei. In the remaining four sources an optical QSO is visible. It is therefore plausible that physical mergers are the most prevalent ULIRG phase, although the optical QSO phase and the IR luminous stage before the galaxies are physically merging in ULIRGs are both significant.

Using *N*-body simulations to assess galaxy–galaxy interactions and mergers has proven to be an invaluable tool (Barnes & Hernquist 1992). The course of a merger event is affected by many variables, including (but not limited to), angle of approach, relative velocity, relative disc inclinations, and gas masses (Barnes & Hernquist 1996). Hence a complete discussion will not be presented here. We instead refer the reader to Barnes & Hernquist (1992). As an example we describe the *N*-body simulations of Dubinski, Mihos & Hernquist (1999), specifically their models A and D. Model A considers a direct coplanar collision between two equal mass galaxies with very low-mass dark matter haloes. After the first close approach at $t = 0$ the galaxies reach a maximum separation of ~ 50 kpc at $t = 2.5 \times 10^8$ yr. After the second close approach at $t \sim 6 \times 10^8$ yr the merger proceeds rapidly and is completed by $t \sim 9 \times 10^8$ yr. The same model but with high mass dark matter haloes (model D) yields a similar pattern of evolution but with a longer merger time of $t \sim 2 \times 10^9$ yr.

Overall, *N*-body simulations of galaxy mergers predict merger times (from first close approach to coalescence) of approximately 10^9 yr. The lifetime of a starburst event has been estimated by several authors. Thornley et al. (2000) find that starburst events are relatively short lived, with a lifetime range of 10^6–10^7 yr, and that galactic superwinds produced by supernovae may be responsible for the short duration. Genzel et al. (1998) derive a starburst age range of 10^7–10^8 yr. Evolutionary models applied to interacting and merging galaxies (Bernloehr 1993) give a starburst lifetime of 2×10^7 yr, but with gaps between starburst events of up to 2×10^8 yr. The lifetime of a ULIRG can be estimated indirectly in two ways, both independent of the power source behind the IR emission. The space density of ULIRGs is approximately the same as that of optically selected QSOs at the same bolometric luminosity in the local Universe (Sanders et al. 1989). If it is assumed that both ULIRGs and QSOs are an event in a host galaxy largely independent of environment then the range in ULIRG lifetimes should be approximately the same as that of QSO lifetimes. Estimating the lifetimes of QSOs is difficult. Recent results (Martini & Weinberg 2001) give a lifetime range of 10^7–10^8 yr. Alternatively the maximum ULIRG lifetime can be estimated by comparing the morphologies in our sample to the *N*-body simulations discussed above. The maximum observed separation in the sample is 30 kpc. Assuming that these galaxies are receding from each other after their first close approach gives a time remaining to merger of 1.6×10^9 yr (model D) or 8.1×10^8 yr (model A). Overall therefore we derive a lifetime range for a ULIRG of approximately 1×10^8–1×10^9 yr. This range is in broad agreement with previous estimates (Murphy et al. 1996), which quote a range of 2×10^8–2×10^9 yr but argue that the real lifetime probably lies towards the lower end of this range.

Clearly there is some discrepancy between these lifetimes. It seems unlikely that ultraluminous IR activity can persist for the entire duration of a merger event, and yet our sample shows ULIRGs at all stages of a galaxy merger. Similarly it seems implausible that a single starburst event can supply the necessary IR luminosity for the entire lifetime of all ULIRGs. On the other hand an AGN cannot be responsible for the IR emission for the majority of the ULIRG phase as most ULIRGs are powered predominantly by starbursts (Genzel et al. 1998; Rigopoulou et al. 1999). To achieve consistency multiple starburst events, similar to those predicted by numerical simulations of multiple galaxy mergers (Bekki 2001) or by previous observations (Murphy et al. 2001), must therefore be invoked before the final merger. Alternatively the evolution of ULIRGs may be more complex than that proposed by Sanders et al., or follow a different pattern.

5.5.2 Starburst and QSO triggering

Starburst triggering in galaxy mergers has previously been examined using numerical simulations where star formation is assumed to follow a density-dependent Schmidt law (Mihos & Hernquist 1994; Mihos & Hernquist 1996). In a merger between two bulgeless disc/halo galaxies it was found that at first perigalacticon bars were formed in each galaxy due to tidal forces, causing a rapid inflow of gas into the central regions. This central gas concentration triggered powerful starbursts as the galaxies reached their maximum separation. This starburst lasts for approximately 10^8 yr, dying out well before the galaxies finally merge at $\sim 10^9$ yr. The ensuing starburst during the merger is very weak. In a merger between two disc galaxies with a significant bulge component the bulges stabilize the galaxies against gas inflow, hence no bars are formed. The resulting starbursts triggered whilst the galaxies are still separate are therefore much less intense than those in bulgeless discs. When the galaxies merge however very large quantities of gas are driven to the central regions of the merger, triggering an extremely intense starburst lasting

$\sim 5 \times 10^7$ yr. A few Gyr after this starburst has ended, the merger remnant strongly resembles a peculiar elliptical galaxy.

Remarkably, these results depend less on orbital dynamics, such as approach angle and relative disc orientation, than progenitor galaxy morphology. The role of orbital dynamics in triggering starbursts is unclear, although the relative orientations of the galaxy discs and the pericentric separation after the first close approach appear important. Direct encounters produce rapid inflows whereas highly inclined passages do not, implying that strong axisymmetric forces are needed for prompt inflows (Barnes & Hernquist 1996). The predicted SFRs also imply that an AGN is not needed to explain the IR emission in ULIRGs. Based on numerical simulations and the then available optical imaging of ULIRGs, Mihos & Hernquist (1996) concluded that most ULIRGs are mergers between disc/bulge/halo systems, with the few ULIRGs composed of widely separated galaxies being mergers between gas rich disc/halo galaxies.

Observations suggest that QSOs contain black holes with mass $> 10^8\,\mathrm{M}_\odot$ (Rees 1984). Spiral galaxies are however thought to contain black holes with mass $\leq 10^7\,\mathrm{M}_\odot$ (Salucci et al. 2000). Although the masses of black holes in ellipticals cover the range $10^7\,\mathrm{M}_\odot < M_{\mathrm{BH}} < 10^{10}\,\mathrm{M}_\odot$ (Magorrian et al. 1998), the quantities of gas and dust in such systems are too small to trigger ultraluminous IR activity in a merger. Hence a $\geq 10^8\,\mathrm{M}_\odot$ black hole must be formed in a galaxy merger if ULIRGs are the transition stage between mergers and QSOs. The formation of quasar nuclei in ULIRGs has been investigated by Taniguchi et al. (1999). They conclude that a supermassive black hole (SMBH) of mass $\geq 10^8\,\mathrm{M}_\odot$ can form if either one of the progenitor galaxies contains a 'seed' SMBH of mass $\geq 10^7\,\mathrm{M}_\odot$ undergoing efficient Bondi type gas accretion over $\sim 10^8$ yr.

5.5.3 *A new picture of ULIRG evolution*

It is apparent from this and previous work that there exist serious problems with the S88 picture. Previous results have highlighted the ambiguity of whether AGN fraction increases with advancing merger stage. Our results are not consistent with ULIRGs being a straightforward transition stage between galaxy mergers and QSOs. Although we find 2/3 warm ULIRGs contain QSOs, our results are not consistent with warm ULIRGs being a transition stage between cool ULIRGs and QSOs.

Our results in conjunction with previous IR spectroscopy and *N*-body simulations (Barnes & Hernquist 1992; Mihos & Hernquist 1994; Mihos & Hernquist 1996; Rigopoulou et al. 1999) lead us to suggest an alternative to the S88 picture. We propose that ULIRGs as a class do not represent a simple transition stage between galaxy mergers and QSOs, and that there exists no sequence from 'cool' ULIRG to 'warm' ULIRG to QSO. Instead we propose that ULIRGs are a much more diverse class of object where the time evolution in IR power source and merger morphology is driven *solely* by the morphologies of the merger progenitors and the local environment. As has been noted by previous authors the presence and size of a bulge component in merger progenitors has a fundamental effect on the timing of gas inflow to the galaxy nucleus. Galaxies with small or non-existent bulge components would starburst early in the merger, galaxies with a large bulge component would starburst late in the merger. It is apparent from our imaging that ultraluminous activity is not mostly confined to late stage mergers and that there exist significant numbers of ULIRGs at all stages in galaxy mergers, including ~ 20 per cent in systems where the galaxies are still separate. This implies that there is a substantial variation in the bulge component over all ULIRG progenitors. This morphological diversity amongst the merger progenitors will give rise to a continuum of starburst and AGN power sources as a function of merger stage across the ULIRG population. The plausible evidence presented here for diversity in environment and hence number of merger progenitors (e.g. pair mergers between field galaxies and multiple mergers between galaxies in compact groups) means that this continuum is more complex than may be expected from just pair mergers. It suggests that there may be a significant variation in the duration and luminosity of the ULIRG phase depending on the local environment. Pair mergers would be ultraluminous in the IR for a shorter period than multiple mergers and have a lower total IR luminosity on average, as there can be more starbursts in a multiple merger. It is worth noting that the combination of violent interaction coupled with large quantities of gas driven to the centres of mergers would undoubtedly increase the chances of forming an AGN and hence an optical QSO. We argue however that the S88 picture represents only a subset of the total ULIRG population described by our model.

To illustrate our alternative model, we describe below three points along this continuum of IR power source as a function of merger stage. Here we only consider pair mergers, as currently no numerical simulations have been performed of multiple galaxy mergers (as may be found in compact galaxy groups rather than in the field) with varying bulge components.

The first point would be a merger between two bulgeless disc/halo galaxies. Starburst activity would be triggered early in the interaction while the galaxies are still separate, largely exhausting the gas supplies in both galaxies and leading to a physical merger that was not ultraluminous in the IR due to a starburst. The early starburst in the progenitors would make accretion commence early in the interaction, possibly leading to an AGN before the galaxies have started to physically merge. The merger would be IR luminous for the first 10^8 yr or so, followed by a quiescent period before (possibly) ending in an IR luminous AGN phase when the galaxies merge. The second point would be a merger between a disc/halo galaxy and a disc/bulge/halo galaxy. A starburst would be triggered in the bulgeless galaxy early in the interaction, and will dissipate before the galaxies start to physically merge. After about 5×10^8 yr, as the galaxies began to physically merge, a starburst would be triggered in the disc/bulge/halo galaxy which had been stabilized against a starburst in the earlier stages of the merger. AGN activity could be triggered both early and late in a merger between two such galaxies. The third point would be a merger between two disc/bulge/halo galaxies. There would be no early starburst and hence no ULIRG activity whilst the galaxies are still separate. Once the galaxies start to coalesce a strong starburst would be triggered. Accretion can only start when the galaxies have started to merge physically. IR luminous AGN activity would probably commence shortly before the end of the starburst phase.

This alternative model resolves many of the problems with the S88 picture highlighted by previous observations. Indeed several observations which directly contradict the S88 picture are in excellent agreement with our model. For example the study showing that the fraction of ULIRGs powered by AGN does not increase with advancing merger stage is in strong agreement with our model, as our model predicts that no such trend should exist. Under our alternative model, starburst and AGN activity could be observed at any point during a merger, depending on the morphologies and local environment of the merger progenitors. As previously noted (Mihos & Hernquist 1994; Mihos & Hernquist

1996) this classification scheme would be largely independent of orbital dynamics.

Although it is not possible with imaging data alone to assign our sample to points along this continuum, we can give examples of typical morphologies at the points described above. A typical 'point 1' object may resemble IRAS 02587−6336. Here the galaxies are still widely separated and hence early in the interaction. There is no QSO activity but the object is ultraluminous in the IR. A 'point 2' object might resemble IRAS 20037−1547. A QSO has been formed in the bulgeless galaxy which formed an AGN early in the interaction due to the early starburst. The source IRAS 18580+6527 is a good example of a 'point 3' ULIRG, where violent star formation has only commenced once the galaxies have started to merge.

An evolutionary track that lasts 10^8–10^9 yr (such as the S88 model or our alternative model) is also testable using other quantities that vary on similar time-scales, or properties that should remain invariant. Observational tests include galaxy morphologies, stellar population mixes and Mpc scale environments. In particular, the QSOs in our sample showed negligible evidence for preferred timing late in the interaction though the number of QSOs in our sample is small. Increasing the number of ULIRG QSOs selected purely on the basis of their FIR emission and observed with very high-resolution imaging would provide better constraints on QSO timing in ULIRGs. Possible theoretical tests include more comprehensive *N*-body simulations of both pair and multiple galaxy mergers, incorporating galaxy morphologies, starburst triggering and QSO formation.

6 CONCLUSIONS

We have presented a sample of 23 ULIRGs, taken with WFPC2 using the F606W band filter on *HST*, and compared this to archival *HST* F814W band data for the same objects. Our conclusions are as follows.

(1) There are no isolated normal spirals or ellipticals in the sample; the sources are either galaxy pairs, merging or interacting systems, or QSOs. The fraction of observed interacting sources in the sample is 87 per cent. As a whole the sample is entirely consistent with ULIRGs being strongly linked with both galaxy interactions and (to a smaller extent) with QSO activity. In three cases, the *HST* images showed clear signs of interaction which had only been ambiguously detected from the ground. Although the majority of the sample are physically merging systems a significant fraction ($\sim$40 per cent) exist in binary systems or QSOs.

(2) Stellar population synthesis models indicate that in most cases the optical emission is dominated by stellar populations with ages of several Gyr or less. Although uncertainties due to unconstrained mass normalizations and dereddening vectors are significant, it seems likely that any optical starburst triggered by interactions does not contribute significantly to the optical emission. The average absolute magnitude for those sources that do not display a QSO is 0.3 mag less bright than the field galaxy magnitude in the Cousins *I* band.

(3) Most of the merging systems in the sample show a number of compact bright 'knots' whose colour differs substantially from the surrounding regions. Colour maps for nine of the objects show a non-uniform colour structure in all but one case. Observed features include blue regions located towards the centres of merging systems, and compact red regions. Although difficult to interpret with only imaging data the blue regions are likely to be regions of enhanced star formation and some of the red regions dust shrouded starbursts or AGN.

(4) There is no apparent correlation between the IR luminosity and either the optical emission or the merger phase for non-QSO ULIRGs. Those ULIRGs that contain a QSO are on average no more symmetrical than those that do not, implying that AGN activity does not tend to reside in more advanced mergers. The relatively small numbers of ULIRGs with a QSO suggest that this phase is short, and although this may be biased by the pre-selected luminosity distribution of the sample, the higher IR luminosity QSOs are if anything over-represented compared to their relative comoving space density. The relatively small number of physically separate objects also suggests that this phase is short and that ULIRGs are dominated by physically merging systems. The QSO host galaxies were found to be either interacting systems or ellipticals. Comparisons between our morphologies and previous merger models suggest that ULIRGs can be both pair mergers between field galaxies and multiple mergers between galaxies in compact groups.

(5) Based on the morphologies of this sample, previous IR spectroscopy, and the results of *N*-body simulations we propose a new model for ULIRG evolution. We propose that ULIRGs are not a simple transition stage between galaxy mergers and QSOs and there exists no sequence from 'cool' ULIRG to 'warm' ULIRG to QSO. Under our model, ULIRGs are an extremely diverse class of object where the time evolution of starburst and AGN activity is driven solely by the morphologies of the merger progenitors and the local environment. This model suggests that the diversity in ULIRG morphologies and the lack of preferred timing of AGN activity in more advanced mergers is due to a continuum of merger progenitor morphologies with varying bulge components. The local environment (field or compact group) affects the number of merger progenitors and hence the frequency and luminosity of starburst events. Although the combination of violent merging and large central gas concentrations would lead to an increased likelihood of AGN activity and as such some ULIRGs would represent such a transition stage, this is only a subset of the ULIRG population as a whole, and there exists no automatic evolution to an optical QSO stage after the ultraluminous IR stage.

ACKNOWLEDGMENTS

We would like to thank Matthew McMaster, Senior Data Analyst at the STScI, for invaluable advice on creating colour maps, and Leon Lucy for help with the deconvolution algorithms. We would also like to thank the referee for his/her very useful comments.

The data presented here were obtained using the NASA/ESA *HST*, obtained at the STScI, which is operated by the Association of Universities for Research in Astronomy, Inc., under NASA contract NAS 5-2655. The work presented has made use of the NASA/IPAC Extragalactic Database (NED), which is operated by the Jet Propulsion Laboratory under contract with NASA, and the Digitized Sky Surveys, which were produced at the STScI under U.S. Government grant NAG W-2166. The images of these surveys are based on photographic data obtained using the Oschin Schmidt Telescope on Palomar Mountain and the UK Schmidt Telescope. D.G.F would like to acknowledge the award of tuition fees and maintenance grant provided by the Particle Physics and Astronomy Research Council (PPARC). This work was in part supported by PPARC (grant number GR/K98728).

REFERENCES

Auriere M., Hecquet J., Coupinot G., Arthaud R., Mirabel I. F., 1996, A&A, 312, 387
Bahcall J. N., Kirhakos S., Schneider D. P., 1996, ApJ, 457, 557
Barger A. J., Cowie L. L., Sanders D. B., 1999, ApJ, 518, L5
Barnes J., 1989, Nat, 338, 132
Barnes J., Hernquist L., 1992, ARA&A, 30, 705
Barnes J., Hernquist L., 1996, ApJ, 471, 115
Bekki K., 2001, ApJ, 546, 189
Bernloehr K., 1993, A&A, 268, 25
Blain A. W., Kneib J.-P., Ivison R. J., Smail I., 1999, ApJ, 512, L87
Borne K. D., Bushouse H., Lucas R. A., Colina L., 2000, ApJ, 529, L77
Boyce P. J. et al., 1998, MNRAS, 298, 121
Brinchmann J. et al., 1998, ApJ, 499, 112
Canalizo G., Stockton A., 2001, ApJ, 555, 719
Caon N., Capaccioli M., D'Onofrio M., 1994, A&AS, 106, 199
Carico D. P., Graham J. R., Matthews K., Wilson T. D., Soifer B. T., Neugebauer G., Sanders D. B., 1990, ApJ, 349, L39
Clements D. L., Baker A. C., 1996, A&A, 314, L5
Clements D. L., Sutherland W. J., McMahon R. G., Saunders W., 1996a, MNRAS, 279, 477
Clements D. L., Sutherland W. J., Saunders W., Efstathiou G. P., McMahon R. G., Maddox S., Lawrence A., Rowan-Robinson M., 1996b, MNRAS, 279, 459
Condon J. J., Huang Z.-P., Yin Q. F., Thuan T. X., 1991, ApJ, 378, 65
Diamond P. J., Goss W. M., Romney J. D., Booth R. S., Kalberla P. M. W., Mebold U., 1989, ApJ, 347, 302
Disney M. J. et al., 1995, Nat, 376, 150
Draper P. W., Scarrott S. M., Tadhunter C. N., 1993, MNRAS, 262, 1029
Dubinski J., Mihos J. C., Hernquist L., 1999, ApJ, 526, 607
Efstathiou G., Ellis R. S., Peterson B. A., 1988, MNRAS, 232, 431
Farrah D., Verma A., Oliver S. J., Rowan-Robinson M., McMahon R., 2001, MNRAS, submitted
Fioc M., Rocca-Volmerange B., 1997, A&A, 326, 950
Genzel R. et al., 1998, ApJ, 498, 579
Grupe D., Wills B. J., Wills D., Beuermann K., 1998, A&A, 333, 827
Harvanek M., Hardcastle M. J., 1998, ApJS, 119, 25
Heckman T. M., Armus L., Miley G. K., 1990, ApJS, 74, 833
Heckman T. M., O'Dea C. P., Baum S. A., Laurikainen E., 1994, ApJ, 428, 65
Hickson P., 1982, ApJ, 255, 382
Hickson P., 1997, ARA&A, 35, 357
Hines D. C., Schmidt G. D., Smith P. S., Cutri R. M., Low F. J., 1995, ApJ, 450, L1
Holtzman J. A., Burrows C. J., Casertano S., Hester J. J., Trauger J. T., Watson A. M., Worthey G., 1995, PASP, 107, 1065
Hughes D. H. et al., 1998, Nat, 394, 241
Joseph R. D., Wright G. S., 1985, MNRAS, 214, 87
Kelson D. D., Illingworth G. D., van Dokkum P. G., Franx M., 2000, ApJ, 531, 184
Kim D.-C., Sanders D. B., 1998, ApJS, 119, 41
Kim D.-C., Sanders D. B., Veilleux S., Mazzarella J. M., Soifer B. T., 1995, ApJS, 98, 129
Kormendy J., Sanders D. B., 1992, ApJ, 390, L53
Krist J., 1995, ADASS, 77, 349
Lawrence A., Rowan-Robinson M., Leech K., Jones D. H. P., Wall J. V., 1989, MNRAS, 240, 329
Lawrence A. et al., 1999, MNRAS, 308, 897
Leech K. J., Rowan-Robinson M., Lawrence A., Hughes J. D., 1994, MNRAS, 267, 253
Lilly S. J., Eales S. A., Gear W. K. P., Hammer F., Le Fevre O., Crampton D., Bond J. R., Dunne L., 1999, ApJ, 518, 641
Low J., Kleinmann D. E., 1968, AJ, 73, 868
Lucy L. B., 1974, AJ, 79, 745
Magorrian J. et al., 1998, AJ, 115, 2285
Martini P., Weinberg D. H., 2001, ApJ, 547, 12
Mihos J. C., Hernquist L., 1994, ApJ, 431, L9
Mihos J. C., Hernquist L., 1996, ApJ, 464, 641
Murphy T. W., Armus L., Matthews K., Soifer B. T., Mazzarella J. M., Shupe D. L., Strauss M. A., Neugebauer G., 1996, AJ, 111, 1025
Murphy T. W., Soifer B. T., Matthews K., Armus L., 2001, ApJ, in press
Peacock J. A. et al., 2000, MNRAS, 318, 535
Perault M., 1987, PhD thesis, Univ. Paris
Pozzetti L., Bruzual A. G., Zamorani G., 1996, MNRAS, 281, 953
Rees M. J., 1984, ARA&A, 22, 471
Rieke G. H., Low F. J., 1972, ApJ, 176, L95
Rigopoulou D., Spoon H. W. W., Genzel R., Lutz D., Moorwood A. F. M., Tran Q. D., 1999, AJ, 118, 2625
Rowan-Robinson M., 2000, MNRAS, 316, 885
Rowan-Robinson M., Crawford J., 1989, MNRAS, 238, 523
Rowan-Robinson M. et al., 1984, ApJ, 278, L7
Salucci P., Ratnam C., Monaco P., Danese L., 2000, MNRAS, 317, 488
Sanders D. B., Mirabel I. F., 1996, ARA&A, 34, 749
Sanders D. B., Soifer B. T., Elias J. H., Madore B. F., Matthews K., Neugebauer G., Scoville N. Z., 1988, ApJ, 325, 74
Sanders D. B., Phinney E. S., Neugebauer G., Soifer B. T., Matthews K., 1989, ApJ, 347, 29
Serjeant S., Mobasher B., Gruppioni C., Oliver S., 2000, MNRAS, 317, L29
Shier L. M., Rieke M. J., Rieke G. H., 1996, ApJ, 470, 222
Soifer B. T. et al., 1984, ApJ, 278, L71
Sopp H., Alexander P., Riley J., 1990, MNRAS, 246, 143
Surace J. A., Sanders D. B., Vacca W. D., Veilleux S., Mazzarella J. M., 1998, ApJ, 492, 116
Surace J. A., Sanders D. B., Evans A. S., 2000, ApJ, 529, 170
Taniguchi Y., Shioya Y., 1998, ApJ, 501, L167
Taniguchi Y., Ikeuchi S., Shioya Y., 1999, ApJ, 514, L9
Thornley M. D., Schreiber N. M., Forster L. D., Genzel R., Spoon H. W. W., Kunze D., Sternberg A., 2000, ApJ, 539, 641
Ulvestad J. S., 1985, ApJ, 288, 514
Uomoto A., Caganoff S., Ford H. C., Rosenblatt E. I., Antonucci R. R. J., Evans I. N., Cohen R. D., 1993, AJ, 105, 1308
Urry C. M., Falomo R., Scarpa R., Pesce J. E., Treves A., Giavalisco M., 1999, ApJ, 512, 88
Vader J. P., Simon M., 1987, Nat, 327, 304
Veilleux S., Kim D.-C., Sanders D. B., Mazzarella J. M., Soifer B. T., 1995, ApJS, 98, 171
Veilleux S., Kim D.-C., Sanders D. B., 1999, ApJ, 522, 113
Wang J., Heckman T. M., Weaver K. A., Armus L., 1997, ApJ, 474, 659
Wilkinson M. I., Evans N. W., 1999, MNRAS, 310, 645
Xia X.-Y., Mao S., Wu H., Zheng Z., Boller Th., Deng Z.-G., Zhenlong Z.-L., 1999, A&A, 341, L13
Yee H. K. C., Oke J. B., 1978, ApJ, 226, 753
Zhenlong Z., Xia X., Deng Z., Su H., 1991, MNRAS, 252, 593

This paper has been typeset from a TEX/LATEX file prepared by the author.